



Computer Methods in Biomechanics and Biomedical Engineering: Imaging & Visualization



ISSN: 2168-1163 (Print) 2168-1171 (Online) Journal homepage: <https://www.tandfonline.com/loi/tciv20>


Fully automatic segmentation of phalanges from hand radiographs for bone age assessment

Shreyas Simu, Shyam Lal, Kunal Fadte & Atteeque Harlapur


To cite this article: Shreyas Simu, Shyam Lal, Kunal Fadte & Atteeque Harlapur (2019) Fully automatic segmentation of phalanges from hand radiographs for bone age assessment, Computer Methods in Biomechanics and Biomedical Engineering: Imaging & Visualization, 7:1, 59-87, DOI: [10.1080/21681163.2017.1416491](https://doi.org/10.1080/21681163.2017.1416491)

To link to this article: <https://doi.org/10.1080/21681163.2017.1416491>

 View supplementary material 

 Published online: 27 Dec 2017.


 Submit your article to this journal 

 Article views: 57

 View Crossmark data 



Fully automatic segmentation of phalanges from hand radiographs for bone age assessment

Shreyas Simu^a , Shyam Lal^a, Kunal Fadte^b and Atteeque Harlapur^c

^aDepartment of Electronics & Communication Engineering, National Institute of Technology Karnataka, Surathkal, India; ^bDepartment of Orthopaedics, Goa Medical College, Bambolim, India; ^cDepartment of Biochemistry, Belgaum Institute of Medical Sciences, Belgaum, India

ABSTRACT

Segmentation of bones from hand radiograph is an important step in automated bone age assessment (ABAA) system. Main challenges in the segmentation of bones are the intensity inhomogeneity caused by the irregular distribution of X-rays and the overlapping pixel intensities between the bone and soft tissue. Hence, there is a need to develop a robust segmentation technique to tackle the problems associated with the hand radiographs. This paper proposes a fully automatic technique for segmentation of phalanges from left-hand radiograph for bone age assessment. The proposed technique is divided into five stages which are pre-processing, extraction of Phalangeal region of interest, edge preservation, segmentation of phalanges and post-processing. Quantitative and qualitative results of proposed segmentation technique are evaluated and compared with other state-of-the-art segmentation methods. Qualitative results of proposed segmentation technique are also validated by different medical experts. The segmentation accuracy achieved by proposed segmentation technique is 94%. The proposed technique can be used for development of fully ABAA of a person for better accuracy.

ARTICLE HISTORY

Received 30 January 2017
Accepted 9 December 2017

KEYWORDS

Hand bone segmentation; bone age assessment; level set function; Phalangeal region of interest (PROI)

1. Introduction

Radiography was the first non-invasive method used to study the internal structure of our body and diagnose various types of illness. It is simple and one of the most widely used imaging methods. The advent of digital image processing methods have boosted the field of diagnostic medicine and increased the accuracy of results obtained. In past few decades, there has been a growing interest in bone age determination by applying digital image processing techniques on hand radiographs. Bone age assessment (BAA) is a procedure to predict the age of a person whose age is unknown. It is a clinical procedure which can also be used to measure the skeletal maturity (bone age). Also, the discrepancy between chronological age and bone age are used for diagnosing any abnormalities in the growth of a child. The commonly used method in clinical practice is matching the left-hand radiograph of the subject with atlas of a left-hand radiograph, an example is the Greulich and Pyle (1959) method (GP), which contains a reference set of normal and standard left-hand radiograph images. Another procedure is the Tanner and Whitehouse-3 (TW3) method, which is more flexible and has been derived from a solid mathematical base. In the TW3 method, a detailed analysis of every bone of left hand is done, which further leads to assigning scores to each bone and the sum of all scores assesses the bone age. In the work of Tanner et al. (2001), maturity evidence is collected from 20 bones consisting of the combination of Radius, Ulna and Short bones (RUS) and carpal bones which are evaluated separately to give RUS score and Carpal score. Tanner and Whitehouse-2 (TW2) method was preceded by TW3, wherein the scores


were given using all 20 bones. GP method is outdated and is based on human judgement, but preferred by pediatricians due to ease of use over the complexity and time-consumed by the TW3 bone assessment process. Automating the TW3 procedure would reduce the complexity and give a second opinion to radiologists and pediatricians while reducing the overall time consumed in assessment.

However, automation of assessment process is obstructed by the presence of non-uniformities in X-ray exposure on the hand bones. This non-uniform exposure is inherent to the radiography which is largely credited to the heel effect. The intensity inhomogeneity is a smoothly varying function of spatial location. The relative brightness of an object placed for X-ray image acquisition is position dependent. According to Behiels et al. (2001) this is due to the fact that image acquisition parameters that affect intensity inhomogeneity differ due to the position of hand from the recording device.

1.1. Motivation

An open document of United Nations Children's Fund UNICEF (2011), shows an estimation of 27 million births take place every year in India. But the birth registration in country is 70%. Hence, around 30% which is approximately 8 million newly born children are not registered within one year of birth. This leads major problems like difficulty in getting access to basic services and protection, child labour, trafficking and child marriage. According to Census of India-2011 (2011), the birth registration is less than 80% in 8 states and 2 union territories in India. The birth registration is around 60% in other developing countries.

CONTACT Shreyas Simu  shreyas.ec14f09@nitk.edu.in

 Supplemental data for this article can be accessed <https://doi.org/10.1080/21681163.2017.1416491>.

Apart from birth registrations there are other applications of BAA in social fields. Without a certified proof, the children are at risk of underage recruitment into armed forces. There is a major problem of early marriage in India before the legal age of 18 years. Children without an official identity proof are vulnerable to judgement as an adult rather than child or juvenile in criminal courts. Submission of fake documents for team selection of under-16 and under-19 age groups for various sports events is also prevalent in many countries. Therefore, a fast, fairly accurate and fully automatic age assessment system would be desirable.

In field of medicine BAA can be used to identify endocrinological problems. According to [Gilsanz and Ratib \(2005\)](#) these problems in youngsters are already evident in many developing and developed countries, varying in scale and intensity for different age groups and sex. The main factors due to which these endocrinological problems arise are the change in lifestyle and eating habits of people. Thus, the above reasons give a great motivation for developing a simple, fast, accurate and fully automatic BAA system.

1.2. Original contributions

The automation of BAA procedure can be divided into four major stages namely, region of interest (ROI) extraction, bone segmentation, feature extraction and classification. In this paper, we focus on first two stages of Automated Bone Age Assessment (ABAA) which are, extraction of the phalangeal region and segmentation of phalanges (short bones) or more commonly known as bones of the fingers. The main contributions of this paper are as follows:

- (1) We have developed a fully automated PROI extraction method. It is fast, accurate and extracts all five phalangeal regions at the same time. The process of extraction is quite simple as it not based on any complex mathematical procedure and follows a simple hierarchical bone localisation technique.
- (2) We propose a fully automated segmentation technique which uses a level set function to delineate the bones from hand radiograph. Anisotropic diffusion is used before undergoing segmentation to preserve the edges and help in segmentation process. Post-processing stage is included to overcome the limitations of level set functions and also tackle the intensity inhomogeneity problem. The proposed technique tackles the heel effect problem or the bias field that is present in radiographs while segmenting the required bones which was not tackled for hand radiographs by researchers.
- (3) We have compared the segmentation results of proposed technique with many other state-of-the-art segmentation techniques which only few researchers had done before. We have done quantitative analysis of the segmentation results using various quality metrics. Such analysis has not been done before in this area of BAA and hand bone segmentation.
- (4) With the help of medical experts, we created ground truth images of the hand radiographs. Medical experts also helped in rating the segmentation results and hence proving the accuracy of work done by our technique.

This paper is organised as follows: Section 2 discusses the previous work. In Section 3, we describe proposed fully automatic ROI extraction and segmentation of phalanges from hand radiographs. In Section 4, we discuss the experimental results and compare the segmentation results of different techniques with the proposed technique using standard quality metrics. Finally, we conclude the work in Section 5.

2. Previous work

Numerous techniques for assessment of bone age have been presented in the literature. Most of the research works deal with the segmentation of certain areas in the hand radiograph and further predicts the bone age. The poor accuracy in extraction of region and segmentation may be caused by the absence of robust pre-processing functions. Inhomogeneity in pixel intensities also poses a major challenge in the segmentation process. The first attempt to automate bone age assessment has been done by [Michael and Nelson \(1989\)](#), which was called as HANDX system. This proposed system was a semi-automated system, where the accuracy was not reasonable. [Manos et al. \(1994\)](#) used region growing and region merging techniques for segmentation of the bones. [Sharif et al. \(1994\)](#) used a derivative of Gaussian (DoG) for pre-processing and segmentation by thresholding, but the results were not promising.

[Pietka et al. \(2001\)](#) proposed epiphyseal-metaphyseal region of interest (EMROI) extraction technique, which also included a good pre-processing unit. Pre-processing steps involved orientation correction and background removal. EMROI extraction has been done by first detecting the phalangeal tip and then step wedge function to extract the fingers. Later gradient function has been used to mark the epiphyseal region. But the thresholding was not good enough to separate out the spongy and the bone tissue. [Pietka et al. \(2003\)](#) further developed an algorithm using k-means clustering algorithm and Gibbs random fields for segmentation. The drawbacks of this technique were that it was slower compared to k-means segmentation and failed if noise was present.

[Park et al. \(2007\)](#) developed a method to extract the epiphysis using horizontal profile. In this paper, first the background has been removed using least squares algorithm and then boundary tracing has been done. Later the central axis of each finger has been estimated using 3rd order polynomial, because of which even if the fingers were slightly curved, the central axis could be estimated. [Giordano et al. \(2007\)](#) developed a semi-automated system for skeletal bone age evaluation. This proposed method was based on derivative of Gaussian (DoG) filtering and adaptive thresholding for enhancement, but it was not feasible for low contrast images. [Liu et al. \(2007\)](#) used particle swarm optimisation (PSO) for template matching from edge set. In this paper, the hand radiograph image was treated with any edge detecting algorithm and then PSO has been used for matching it to the edge set. [Lee and Kim \(2008\)](#) proposed an EMROI extraction method for the TW2 system in which the boundary was removed using least squares algorithm and later long axis of each finger was extracted. EMROI have been localised by studying the intensity profile along the axis.

[Chai et al. \(2011\)](#) proposed to use gray-level co-occurrence matrix along with k-means for segmentation of bones, but the

results were very poor. Also [Chai et al. \(2013\)](#) used modified histogram enhancement technique for pre-processing. The technique called as multi-objective beta-optimised bi-histogram equalisation has been designed which uses multi-objective optimisation technique for histogram equalisation. [Hsieh et al. \(2012\)](#) have focused on phalangeal region of interest (PROI) extraction using projection profile of the fingers and gamma parameter enhancement has been done. Authors compared the results with and without gamma enhancement for two popular segmentation techniques namely k-means algorithm (KMS) and GVF snakes.

Recently researchers [Güraksin et al. \(2016\)](#) have worked on morphological operators for pre-processing, segmentation and feature extraction. In this paper, authors have used support vector machines (SVM) for classification and their main work was focused on carpal bones and radius bone only for an age group of 0–6 years. [Seok et al. \(2016\)](#) have extracted 17 ROI's altogether from phalanges and radius, ulna bones and used multi-layered fuzzy classifiers for classification. [Spampinato et al. \(2017\)](#) used convolutional neural networks for classification applied directly on the whole radiograph. [Kashif et al. \(2015\)](#) used Scale Invariant Feature Transform (SIFT) feature extraction for BAA and later [Kashif et al. \(2016\)](#) proved that SIFT is better than other feature extraction techniques like BRISK, FREAK, etc. But the authors use a semiautomatic procedure involving thresholding by [Otsu \(1979\)](#) as the main segmentation technique.

There are some state-of-the-art segmentation techniques which haven't been used for phalangeal segmentation. In our previous paper ([Simu and Lal 2017](#)), we have done a detailed study of evolutionary and non-evolutionary segmentation techniques on hand radiographs. In this paper, we have compared recent state-of-the-art segmentation techniques and were applied on the whole hand. Out of those, two recent algorithms in the field of image segmentation have been used for comparison, which are Adaptively Regularised Kernel-based Fuzzy C-means clustering (ARKFCM or AKFM) by [Elazab et al. \(2015\)](#) and Biconvex Fuzzy Variation algorithm (BFV) by [Gong et al. \(2015\)](#). The ARKFCM algorithm (AKFM) is a modified version of fuzzy C-means algorithm, wherein an adaptive regularisation parameter is used to enhance segmentation robustness. It also makes use of weighted image and adopts the Gaussian radial basis function for better accuracy. The BFV algorithm combines fuzzy logic with Chan-Vese (CV) model. CV model given by [Chan and Vese \(2001\)](#) belongs to the class of Partial Differential Equation model equations for solving image segmentation problems. The major problems with CV model are convergence to local optima, highly dependent on parameter selection, and computationally expensive. The BFV algorithm overcomes these problems by efficiently combining numerical remedy techniques. This, in turn, reduces the computational costs and brings a lot of robustness to parameter settings. In order to improve the accuracy of automated bone age assessment, a new ROI extraction method and improved segmentation technique is proposed for segmentation of hand radiographs.

In this paper, effective fully automatic technique for segmentation of phalanges from hand radiograph is proposed. Through extensive simulation results, it is clear that many of the existing state-of-the-art segmentation methods fail to yields better seg-

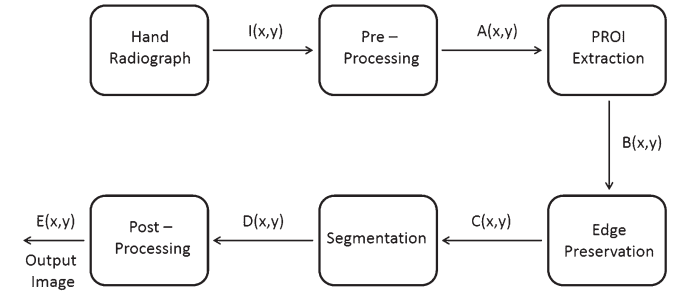


Figure 1. Block diagram of the proposed fully automatic ROI extraction and segmentation of phalanges.

mentation results. The proposed technique has been shown to outperform the existing state-of-the-art segmentation methods.

3. Proposed fully automatic segmentation technique

In this section, a detailed mathematical analysis of a proposed fully automatic ROI extraction and segmentation of phalanges from hand radiographs are presented. The proposed technique for segmentation of phalanges consists mainly of five main stages which are, (1) Pre-processing of the left-hand X-ray image, (2) Extraction of the PROI, (3) Edge Preservation, (4) Segmentation of the bones in PROI, (5) Post-processing of the segmented image. The schematic diagram of the proposed technique is shown in Figure 1.

The pre-processing stage involves noise removal and readying of hand radiograph for ROI extraction stage. Let the output image after this stage be called as A . The next step is the extraction of PROI. Let the extracted image be B . Edge-preservation operation is performed on extracted image using anisotropic diffusion to give an output image C . The next stage is segmentation of bones in PROI which gives image D . Segmented image D is further post-processed and the end result is given in image E . Due to the presence of non-uniformly distributed X-ray intensities, segmentation step is followed by post-processing stage to increase the segmentation accuracy. This stage also removes any vestigial regions that might be present after segmentation stage. Further, the detailed description of each block is described as follows:

3.1. Pre-processing of hand radiograph

It is important to prepare the image before we start the extensive procedure of extraction of PROI followed by segmentation. For efficient and accurate ROI extraction from the radiograph of left hand, it is subjected to Gaussian filtering as given by [Gonzalez and Woods \(2004\)](#). The Gaussian filter removes the noise present in the hand radiograph image to give resultant image A . The filter has a Gaussian profile which is convolved with the image and is given in Equation (1)

$$A(x, y) = I(x, y) * L(x, y), \quad (1)$$

where $I(x, y)$ is the input radiograph image and Gaussian filter is defined by $L(x, y) = \frac{1}{2\pi\sigma^2} e^{-\frac{x^2+y^2}{2\sigma^2}}$. In the above equation $*$ stands for convolution and σ is the standard deviation.

3.2. PROI extraction

After studying the shape and structure of fingers, the extraction of PROI is done with the help of morphological operators. The steps are as follows:

- (1) Multi-level [Otsu \(1979\)](#) thresholding to get the boundary of hand.

$$\sigma_w^2(t_h) = \omega_1(t_h)\sigma_1^2(t_h) + \omega_2(t_h)\sigma_2^2(t_h) \quad (2)$$

where $\omega_i(t_h)$ stands for probabilities of two classes ($i = 1, 2$) separated by a threshold t_h . In this paper [Otsu \(1979\)](#), has shown that minimising the intra class variance $\sigma_w^2(t_h)$ is same as maximising the inter-class variance $\sigma_b^2(t_h)$.

- (2) Morphological erosion to smoothen the boundary of hand. The erosion of input image A after thresholding is done by structuring element S is given by equation:

$$A \ominus S = x : S_x \subset A \quad (3)$$

where \subset denotes subset. $A \ominus S$ is made up of all the points x for which the translation of S by x fits in A as given by [Dougherty and Lotufo \(2003\)](#).

- (3) Edge-off and area-opening function to remove any unnecessary objects present in the image. [Dougherty and Lotufo \(2003\)](#) define edge-off function as process of removing any object that is connected to edge of the image and area opening function or area open filter removes an object from the image, if it's size is less than some value ν , then

$$A \circ (\nu)_n = \bigcup Q, \text{area}(Q) \geq \nu \quad (4)$$

where A is the binary image and Q is the area of n -connected component.

- (4) Skeleton function and thinning operation to get the skeleton of binary image. Skeleton of the binary image is formed by centres of all the maximal discs. A maximal disc is any disc such that there does not exist any other disc within the image containing the given disc.
- (5) Use region properties function to find bounding box, orientation and area of all skeletons.
- (6) Using the derived region properties draw a rectangular box around the phalanges and crop the region to get the PROI image $B(x, y)$.

3.3. Edge preservation

Prior to the segmentation of bones in PROI, an anisotropic diffusion has been applied for edge preservation. [Perona and Malik \(1990\)](#) introduced anisotropic diffusion, also known as non-linear anisotropic diffusion. Unlike other isotropic diffusion algorithms used for noise removal, anisotropic diffusion algorithm preserves the edges while diffusing the noise. Assume $B(x, y)$ is the input image. Let $G(x, y)$ be the diffusion function. The equation given by Perona and Malik is:

$$\frac{\delta(B(x, y, t))}{\delta t} = \text{div}(G(x, y, t)\nabla(B(x, y, t))) \quad (5)$$

where $\nabla(B)$ is the image gradient and t denotes time step. The diffusion function depends on the image gradient magnitude $\|\nabla(B)\|$. [Hum \(2013\)](#) states that, for larger gradient values the diffusion is low and for smaller gradient values the diffusion is high. The anisotropic diffusion preserves the edges by smoothing the texture inside the object and sharpening the edges of the object. Two diffusion functions have been proposed by [Perona and Malik \(1990\)](#):

$$G(x, y, t) = \exp\left(-\left(\frac{\|\nabla(B(x, y, t))\|}{\lambda}\right)^2\right) \quad (6)$$

$$G(x, y, t) = \frac{1}{1 + \left(\frac{\|\nabla(B(x, y, t))\|}{\lambda}\right)^{1+a}} \text{ where } a > 0 \quad (7)$$

λ is a constant which is used to control the diffusion strength. The first equation of anisotropic diffusion with λ value set to the variance of the image has been considered in this study and the output of this stage is image $C(x, y)$.

3.4. Segmentation of bones in PROI

The segmentation of pre-processed PROI images has been carried out using the level set concept given by [Osher and Sethian \(1988\)](#) and then followed by post-processing operations. The reason for selecting level set method for segmentation purpose is that it follows shapes and curves very easily even the ones with holes or dents. It is very much suitable for capturing the shape of bones which are touching each other. The detailed analysis of segmentation of pre-processed PROI images is explored in this section. Let pre-processed PROI image C which is extracted from hand radiograph can be modelled by the following equation:

$$C = bZ + n \quad (8)$$

where Z is the true image, b is the bias field due to heel effect and n is the additive noise. True image Z is the depiction of physical characteristics of hand. The image C is a function $C : \Omega \rightarrow R$ defined on the continuous domain Ω . The bias field is assumed to be smoothly varying. The true image Z can be divided into N different regions $\Omega = \bigcup_{i=1}^N \Omega_i$. Each of this region takes a constant value p_1, p_2, \dots, p_N .

Consider a centre point c of a circular area with radius r , c belongs to Ω , $V_c = \{x : |x - c| < r\}$. If we divide Ω into N regions $\Omega_{i=1}^N$, this will divide the circular area $V_c \cap \Omega_i$ as defined by [Li et al. \(2011\)](#). From Equation (8) and the above formulation is given in Equation (9):

$$C(x) = b(x)p_i + n(x) \text{ for } x \text{ belongs to } V_c \cap \Omega \quad (9)$$

The segmentation of bones can be achieved by minimising the following energy function:

$$W(b, Z) = \int_{\Omega} |C(x) - b(x)Z(x)|^2 dx \quad (10)$$

which can be further written as:

$$W(b, p) = \int_{\Omega} |C(x) - b(x)p_i|^2 dx \quad (11)$$

Level set function defined by [Osher and Sethian \(1988\)](#) can now be used to minimise this energy function as given by CV model of [Chan and Vese \(2001\)](#).

$$F(b, p, \phi) = \int_{\Omega} |C(x) - b(x)p_1|^2 H(\phi(x)) dx + \int_{\Omega} |C(x) - b(x)p_2|^2 (1 - H(\phi(x))) dx + \mu \int_{\Omega} |\nabla H(\phi(x))| dx \quad (12)$$

where H is the Heaviside function and ϕ is the level set function. This level set function divides the image into two regions $\Omega_1 = \{x : \phi(x) < 0\}$ and $\Omega_2 = \{x : \phi(x) > 0\}$. The first two terms in the Equation (12) are data fitting terms, whereas the last term regularises the zero level contour as defined by [Osher and Sethian \(1988\)](#). Therefore, the image segmentation is achieved by finding the level set function ϕ , bias field b and the constants p_1 and p_2 that minimise the energy function F .

Let u_i denote the membership function for the regions Ω_i . If we want to divide the image into object and background we define $u_1(\phi) = H(\phi)$ and $u_2(\phi) = 1 - H(\phi)$, where H is the Heaviside function. Now the energy function can be written as:

$$W(b, p, \phi) = \int_{\Omega} \sum_{i=1}^N |C(x) - b(x)p_i|^2 u_i(\phi(x)) dx \quad (13)$$

Now this energy term is used as data term in Equation (12) and the equation is rewritten as:

$$F(b, p, \phi) = W(b, p, \phi) + \mu R(\phi) \quad (14)$$

where μ is the weight and $R(\phi)$ is the regularisation term which is equal to $\int_{\Omega} |\nabla H(\phi(x))| dx$. The minimisation is achieved by performing iterations, where in each iteration we fix any two variables and minimise the Equation (14) with respect to the third variable. By minimising this energy function with respect to each of these variables b , p and ϕ , we can segment the bones from PROI. The output image of segmentation stage is $D(x, y)$ which is the input for post-processing stage. The minimisation steps are described as follows:

- (1) Energy minimisation with respect to ϕ : For fixed values of p and b the minimisation of $F(b, p, \phi)$ can be achieved using gradient descent method.

$$\frac{\partial \phi}{\partial t} = -\frac{\partial F}{\partial \phi} \quad (15)$$

Using calculus of variations we have:

$$\frac{\partial \phi}{\partial t} = -\delta(\phi)(d_1 - d_2) + \mu \delta(\phi) \operatorname{div} \left(\frac{\nabla(\phi)}{|\nabla(\phi)|} \right) \quad (16)$$

where $d_i = \int |C(x) - b(x)p_i|^2 dx$ and $i = 1, 2$.

- (2) Energy minimisation with respect to p : For fixed values of ϕ and b , the optimised value of p can be denoted as:

$$p'_i = \frac{\int bC(x)u_i(\phi(x))dx}{\int b^2u_i(\phi(x))dx} \text{ where } i = 1, 2 \quad (17)$$

- (3) Energy minimisation with respect to b : For fixed values of ϕ and p , the optimised value of b can be denoted as:

$$b' = \frac{C(x)[(p_1u_1(\phi(x))) + (p_2u_1(\phi(x)))]}{[(p_1^2u_1(\phi(x))) + (p_2^2u_1(\phi(x)))]} \quad (18)$$

3.5. Post processing

This step is necessary for the procedure to extract accurate information from the segmented bones because sometimes the contours which are initialised by level set function to track the bone edges might not behave in the required way. This is due to either or both of the following reasons:

- (1) It tracks the cancellous bone region along with the cortical bone region. Cancellous bone is also known as the trabecular bone which is soft osseous tissue that forms the internal bone, whereas cortical/compact bone forms the exterior part of bone.
- (2) Due to intensity inhomogeneity and overlapping pixels between bone and soft tissue, the tissue region also gets identified as an object of interest.
- (3) The level set function develops some irregularities during its evolution as mentioned by [Li et al. \(2011\)](#).

To mitigate these errors, morphological operators have been used in the post-processing operation. The post processing steps are involved as follows:

- (1) Image filling function along with erosion and dilation operations. The dilation of any binary image D by structuring element S is given by [Dougherty and Lotufo \(2003\)](#):

$$D \oplus S = (D' \ominus S^*)' \quad (19)$$

The dilation of D by S is done by rotating S around origin to get S^* and then D' which is a complement of D is eroded by S^* .

- (2) Area opening function along with erosion and dilation operations. The equations for these operations are given in Equations (3), (4) and (19).
- (3) Edge off function to remove any unnecessary objects or other bone parts that might be present at the boundary of PROI.

All the functions and operators used in pre and post-processing operations are applied from morphology toolbox defined by [Dougherty and Lotufo \(2003\)](#). The output image of this final stage is $E(x, y)$.

3.6. Implementation of proposed technique

The implementation steps of proposed fully automatic ROI extraction and segmentation technique are given as follows:

- (1) **Noise removal:** The first step is pre-processing, where Gaussian low pass filtering has been used for noise removal as given in Equation (1). The filter size is 3×3 with sigma value set to 5. Please note that hand radiographs are not resized.
- (2) **Boundary extraction:** The PROI extraction stage begins with multi-level Otsu thresholding to extract the bound-

ary of hand. Matlab function *multithresh* and morphology toolbox function *mmthreshad* are used to perform this operation. Now we have a binary image after the previous step of thresholding. Smoothen the boundary of hand in radiograph using erosion operation *mmero* as given in the Equation (3). Structuring element used here is cross with size 2. Please note that functions starting with *mm* are morphology toolbox functions and rest are Matlab functions.

- (3) **Superfluous object removal:** Unnecessary objects present in the image are removed using *mmedgeoff* and *mmareaopen* functions.
- (4) **PROI extraction:** The skeleton of hand is extracted using *mmskelm*, *mmthin*, *mmendpoints* functions and then labelled using *bwlabel* function. These labelled objects are further processed using *regionprops* function to extract information and then cropped to get the PROI from hand radiograph. We used orientation option from *regionprops* function to align the PROI's vertically.
- (5) **Anisotropic Diffusion:** Anisotropic diffusion algorithm has been used to preserve the edges present in the image. Time step t in Equation (5) is set to 5 and the value of λ in Equation (6) is made equal to variance of the image.
- (6) **Initialisation of level set function:** Initialisation of level set contour on the image has been done randomly. As we found that contours initialised in a shape of box or circle get trapped in a region and are not able to proceed further. The Heaviside function H used during implementation is the smoothed version of Heaviside function and is defined as Osher and Sethian (1988):

$$H_\nu(x) = \frac{1}{2} \left[1 + \frac{2}{\pi} \arctan \left(\frac{x}{\nu} \right) \right] \quad (20)$$

where $\nu = 1$.

- (7) **Energy minimisation:** For energy minimisation the weight of regularisation term μ in Equation (14) is set to any smaller value. We have found it to be best if it is made equal to the standard deviation of the extracted ROI image. Energy minimisation is achieved using the equations (16), (17) and (18). The number of iterations is set to 100.
- (8) **Post-processing:** The functions used for post processing are image filling function *imfill* and dilation operation *mmdil*. Area-opening and edge-off functions may be used to remove unnecessary bone parts present in the ROI.

3.7. Illustration of proposed technique

In this section, we will illustrate the proposed technique in a stepwise manner with the help of output images from each stage. From the theory explained in Section 3, we can say that the proposed technique is divided into stages which are, PROI extraction, edge-preservation (Pre), segmentation (Seg) and post-processing (Post) stages. We have illustrated the stage-wise results in Figures 2–6, which shows the implementation of proposed technique on hand radiographs of ages 1, 5, 10, 12 and 16-year-old person, respectively. The visual results for pinky, ring, middle, index and thumb fingers have been shown in Figures

2–6. Quantitative results of each stage have been evaluated and compared in terms of quality metrics like PSNR, MSE, SSIM, which are given in the Table 1. Results in Table 1 show considerable improvement in values of quality metrics after every stage. Please note that the output image after an edge-preservation stage is compared with PROI image where both are grayscale images, whereas the output images of other two stages are compared with ground truth image in which all images are binary. It can be noticed that there was a considerable improvement at each stage of proposed technique and the final output image is similar to ground truth image. The advantages of proposed technique are: (1) It is very effective and robust as it tackles intensity inhomogeneity problem in hand radiographs. (2) It clearly delineates phalanges from hand radiographs of different ages which make it easier for further assessment. (3) It successfully removes all spurious regions and achieves higher segmentation accuracy. The main drawback of proposed technique is that it consumes more time compared to other state-of-the-art segmentation techniques.

4. Experimental results and discussion

In this section, we have presented experimental results and also discussed the performances of different segmentation techniques on digital hand radiographs with age group 0-18 years. The experimental results of proposed fully automatic segmentation technique is evaluated and compared with other state-of-the-art segmentation techniques such as Otsu's thresholding by Otsu (1979), KMS by Hartigan and Wong (1979), k-means with Gibb's random fields (KGRF) by Pappas and Jayant (1988), PSO based segmentation algorithm (PSO) by Eberhart and Kennedy (1995), AKFM developed by Elazab et al. (2015) and BFV algorithm (BFV) by Gong et al. (2015). The state-of-the-art segmentation techniques considered for comparison are popular and widely used on hand radiographs. The KGRF segmentation technique has been used by many researchers in the field of BAA like, Pietka et al. (2003), Gertych et al. (2007), Trist-Vega and Arribas (2008) and Giordano et al. (2010), which was based on adaptive clustering method coined in the paper of Pappas and Jayant (1988). The PSO based segmentation algorithm was also used by many researchers in this field like Liu et al. (2007) and Thangam et al. (2012). In all state-of-the-art segmentation techniques we include pre-processing and edge preservation step as used in proposed segmentation technique. All simulation results have been obtained on a 64-bit system with MATLAB 2015a software, having a 8 GB RAM and an Intel i7 processor with clock speed of 3.6 GHz.

4.1. Image database

The database used for the experimentation has been acquired from an online website, <http://www.ipilab.org/BAAweb/>. The images on this website have been collected from Children's Hospital Los Angeles, USA (Gertych et al. 2007). The manual segmentation or ground truth images were constructed with the help of medical experts from Goa Medical College, Bambolim, Goa, India for analysis of obtained segmentation results.

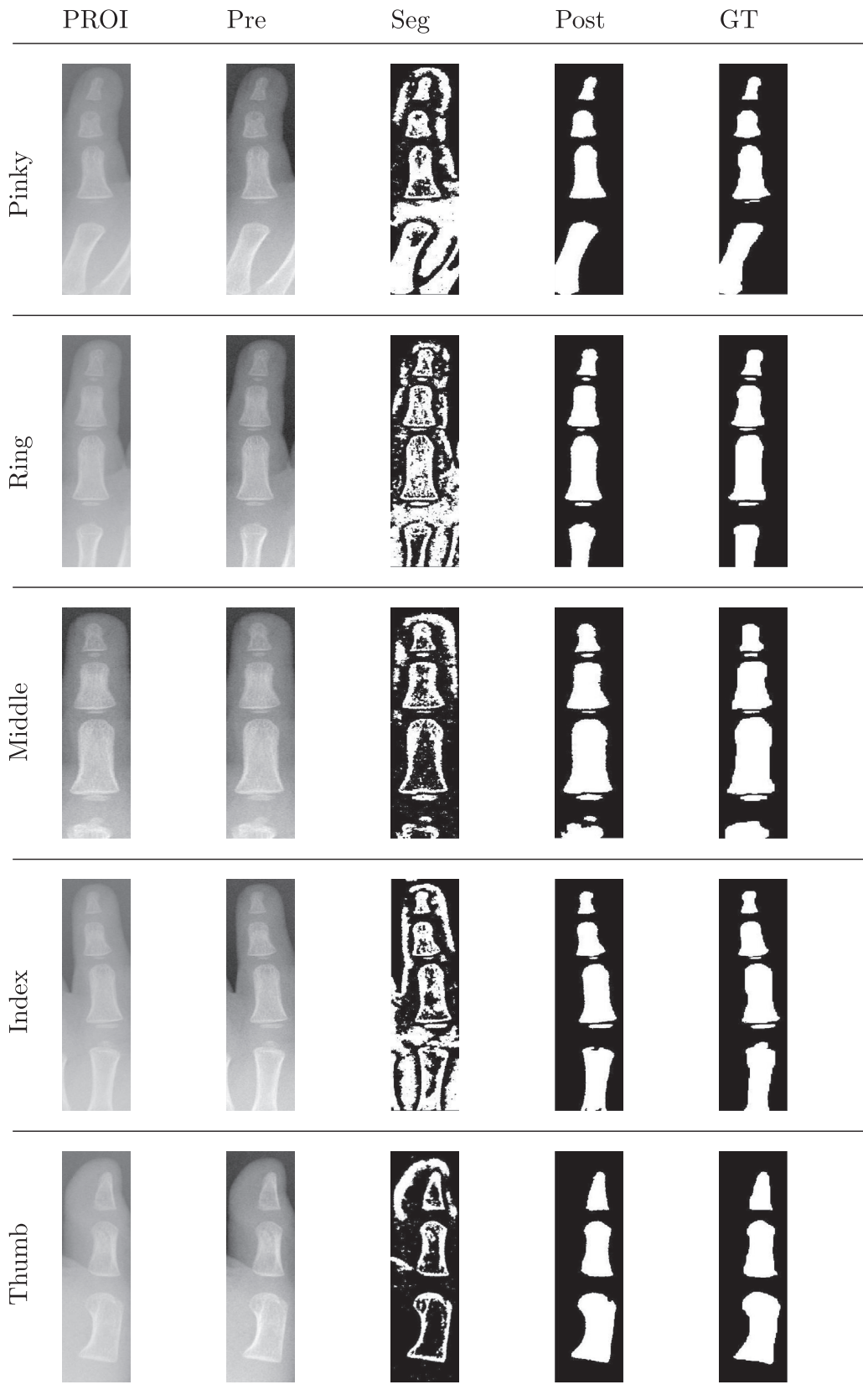


Figure 2. Output images from each stage of the proposed technique on hand radiograph of 1 year old person [5173.jpg].

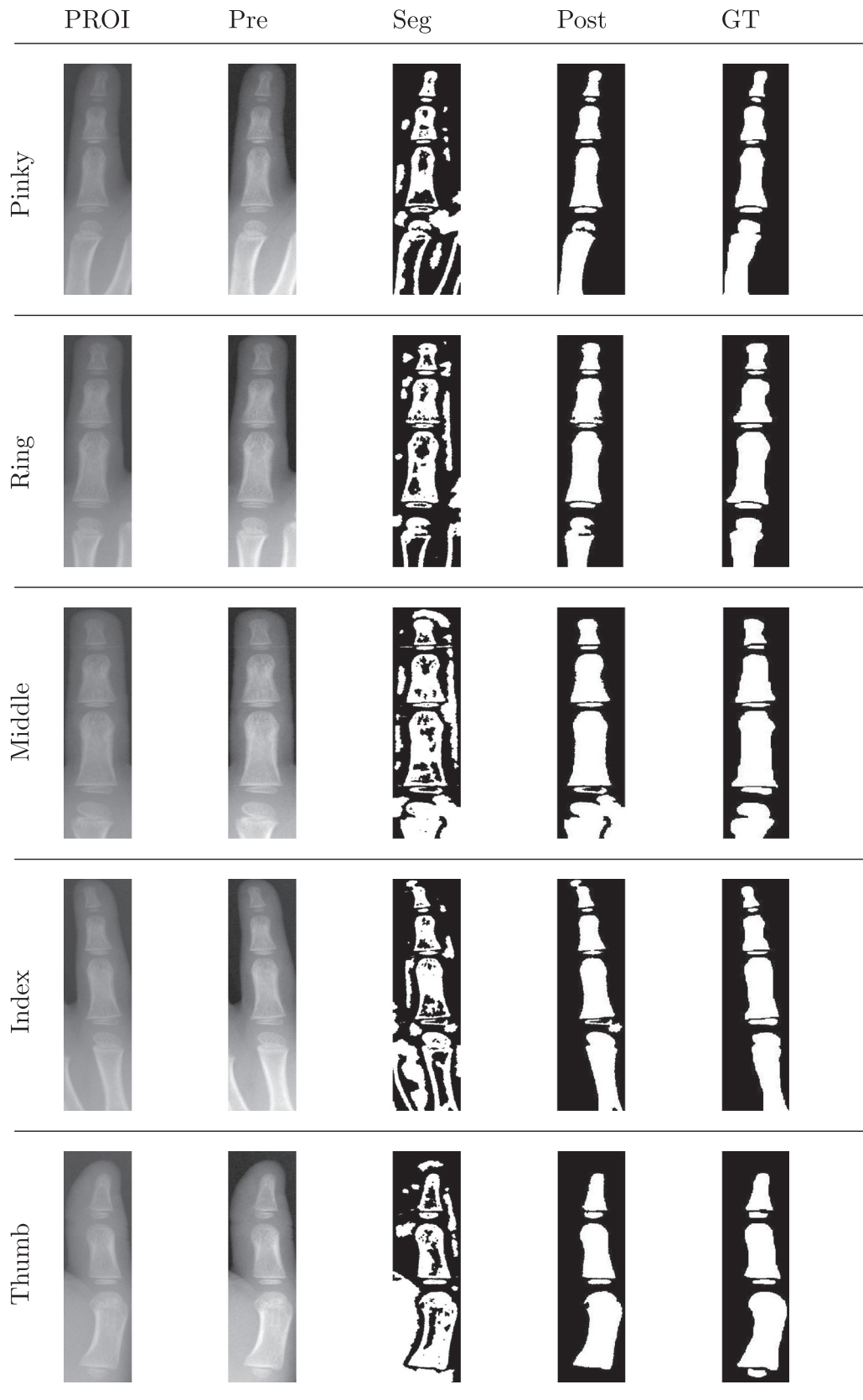


Figure 3. Output images from each stage of the proposed technique on hand radiograph of 5 year old person [7143.jpg].

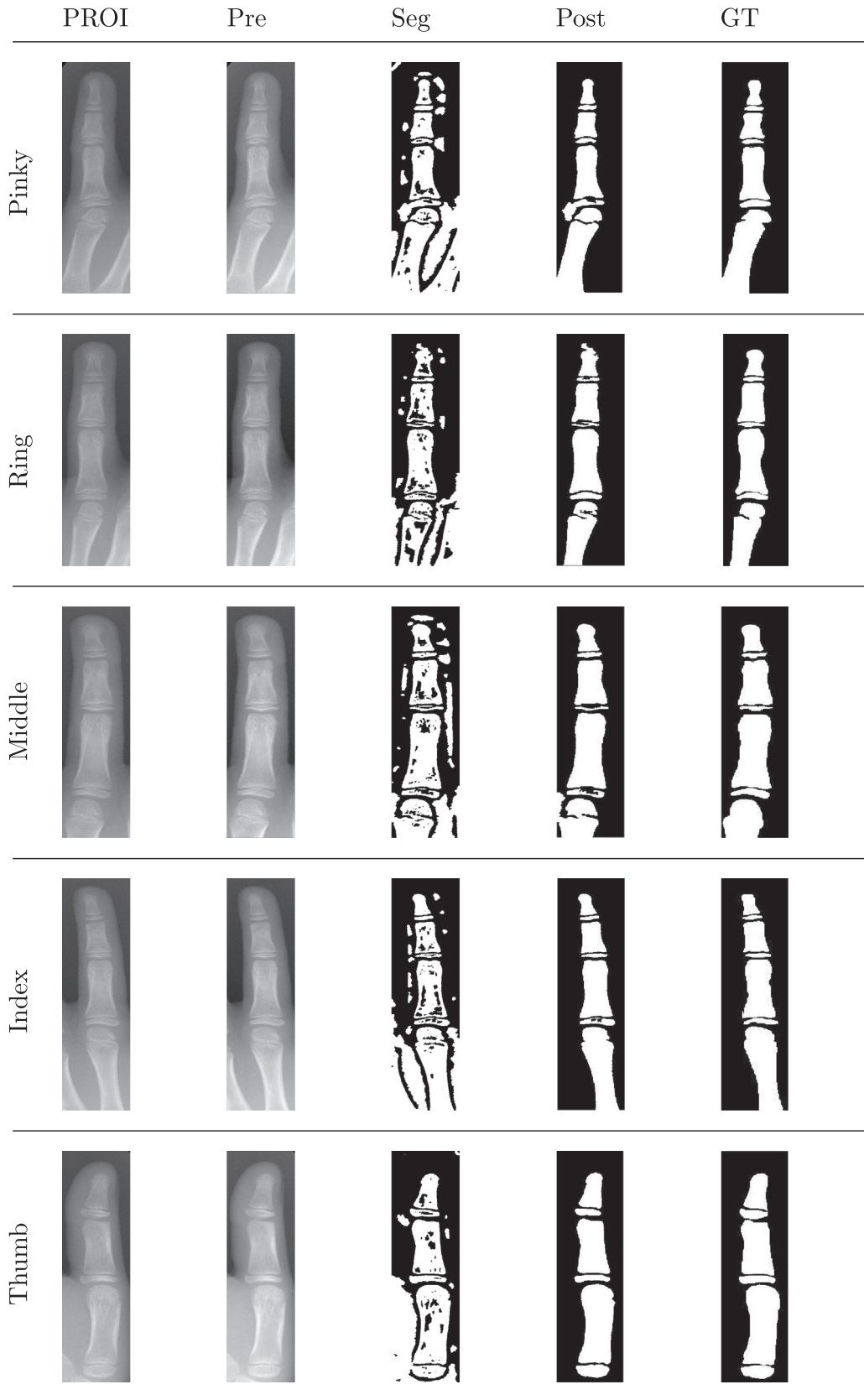


Figure 4. Output images from each stage of the proposed technique on hand radiograph of 10 year old person [5113.jpg].

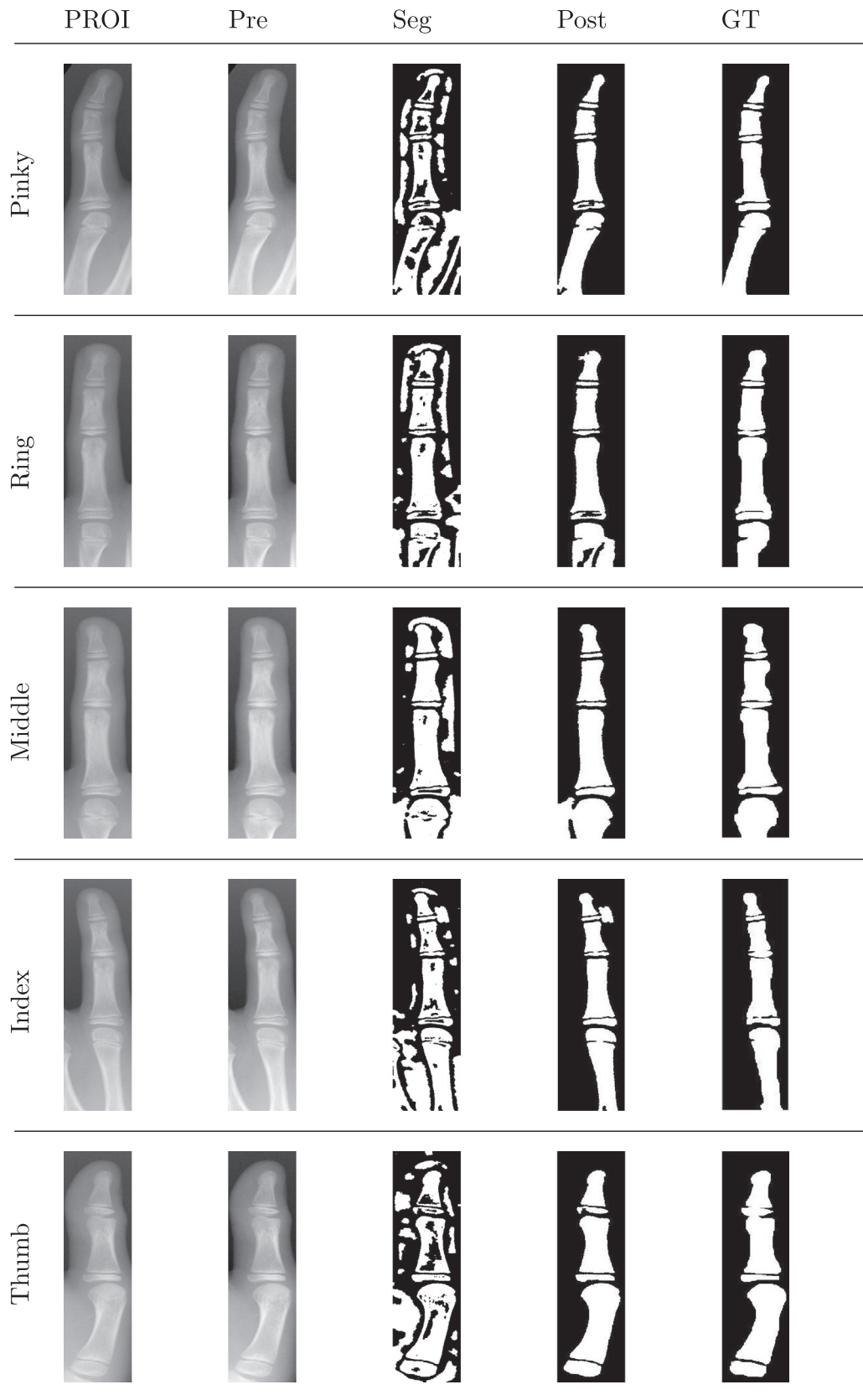


Figure 5. Output images from each stage of the proposed technique on hand radiograph of 12 year old person [5322.jpg].

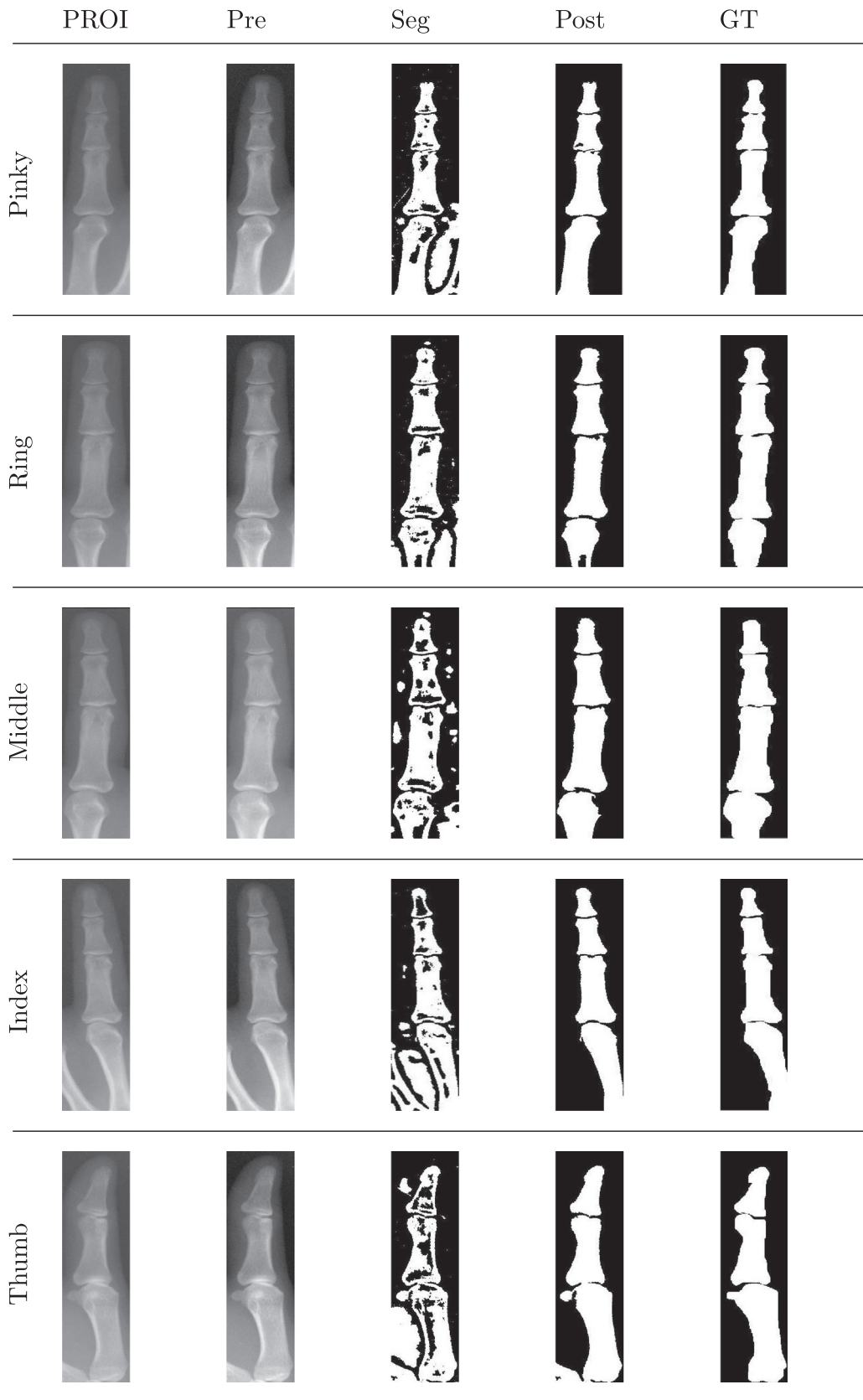


Figure 6. Output images from each stage of the proposed technique on hand radiograph of 16 year old person [5257.jpg].

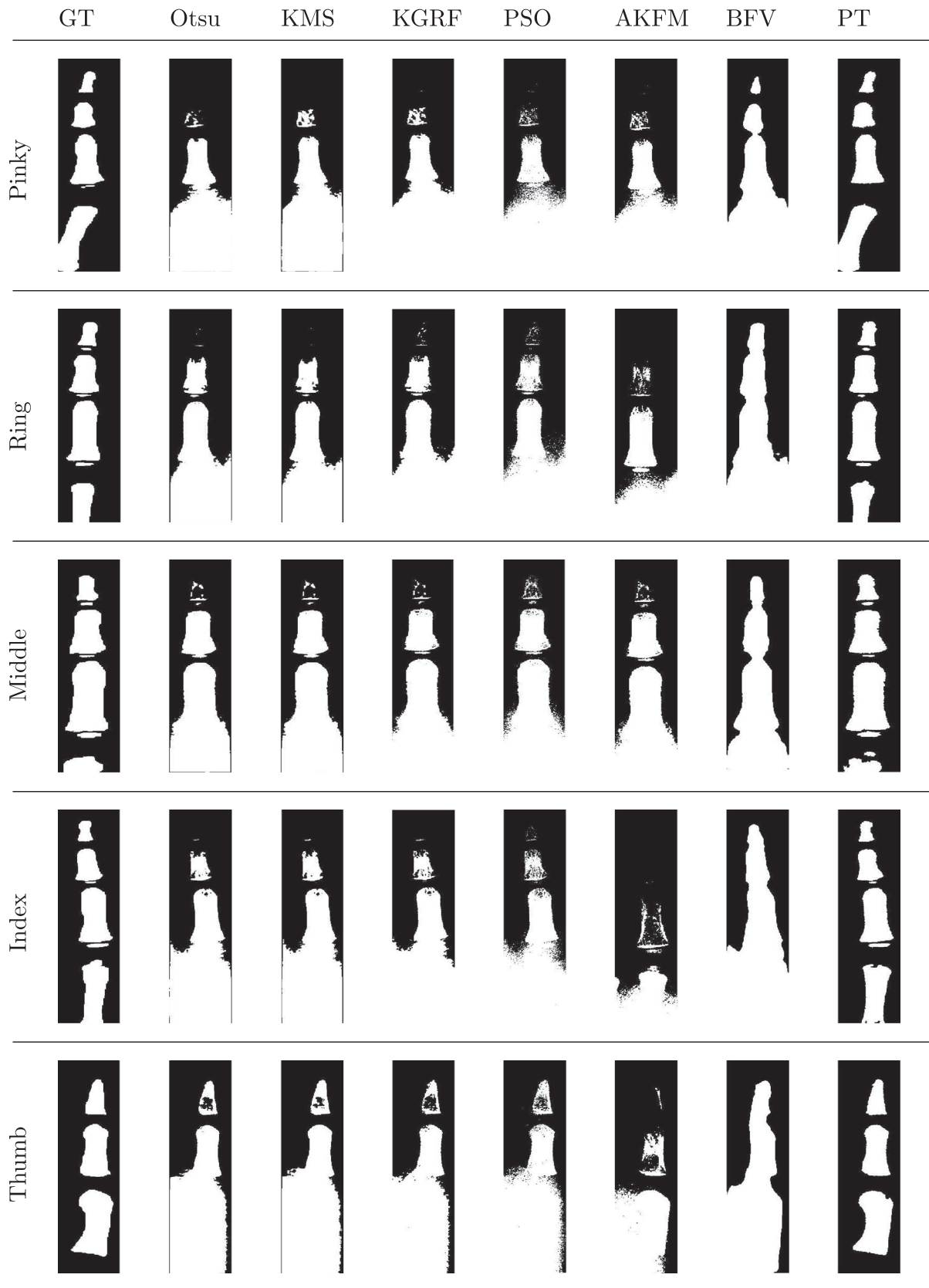


Figure 7. Segmentation results of different algorithms on hand radiograph taken from 1 year old person [5173.jpg].

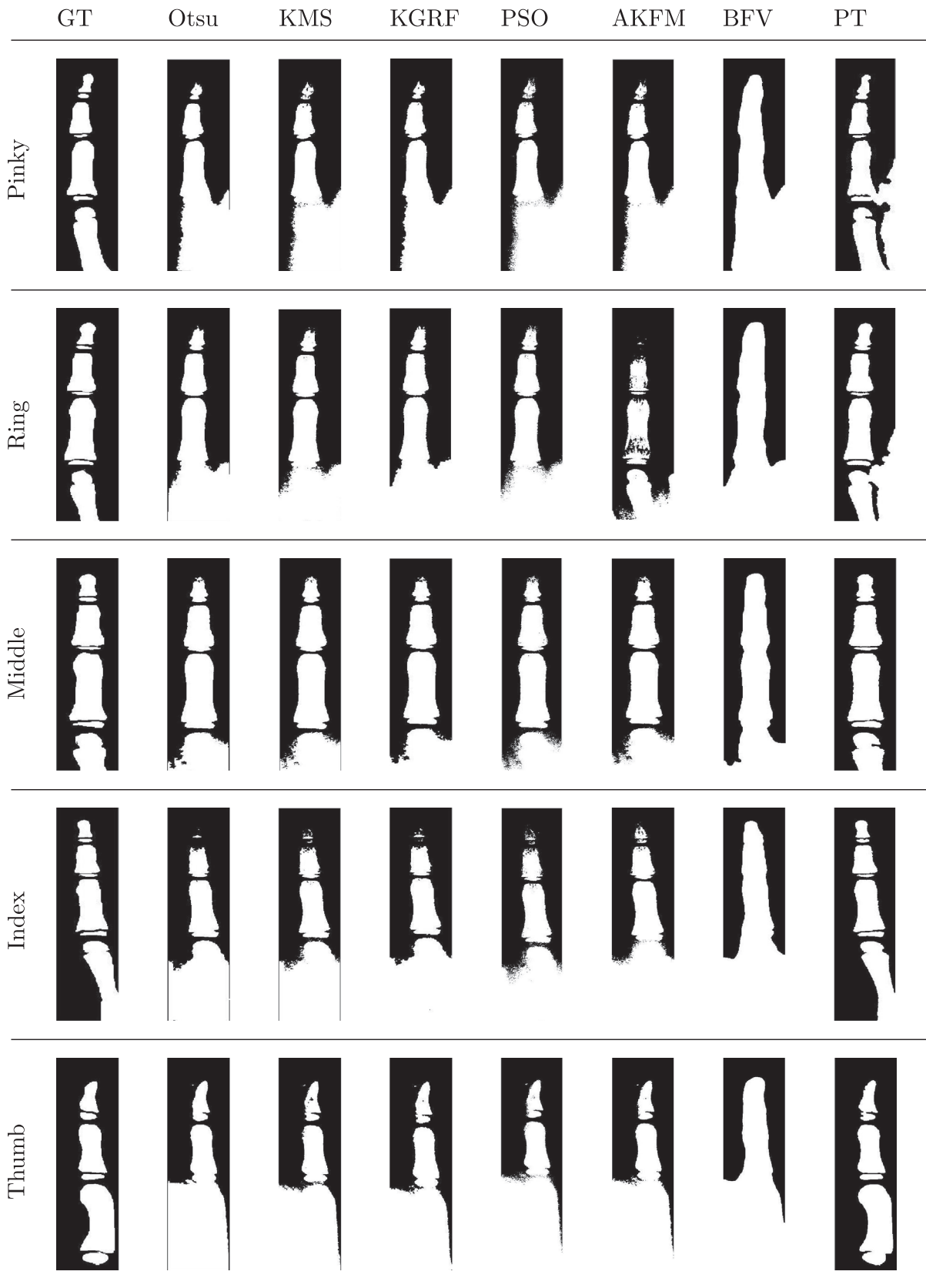


Figure 8. Segmentation results of different algorithms on hand radiograph taken from 3 year old person [6102.jpg].

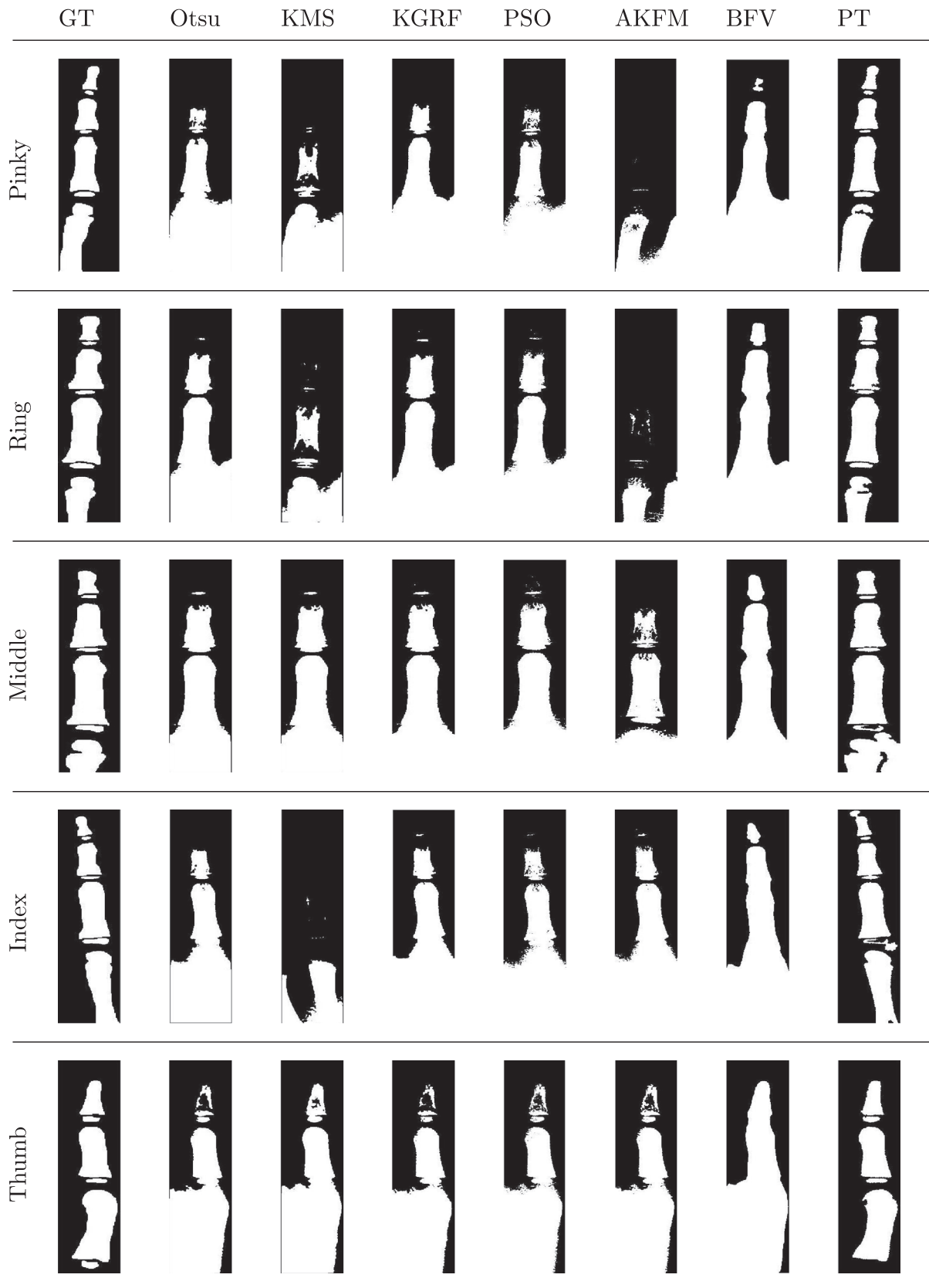


Figure 9. Segmentation results of different algorithms on hand radiograph taken from 5 year old person [7143.jpg].

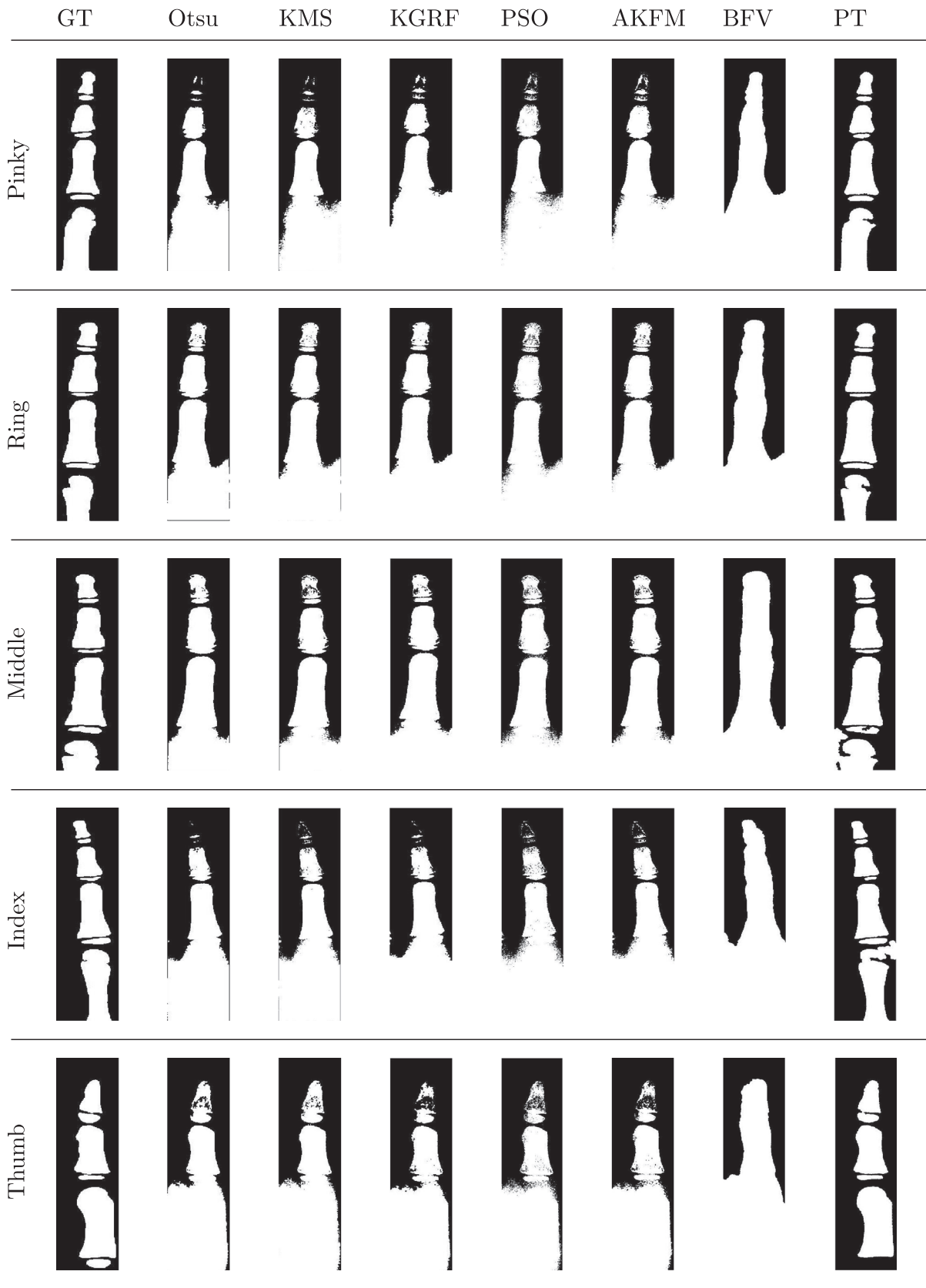


Figure 10. Segmentation results of different algorithms on hand radiograph taken from 7 year old person [5154.jpg].

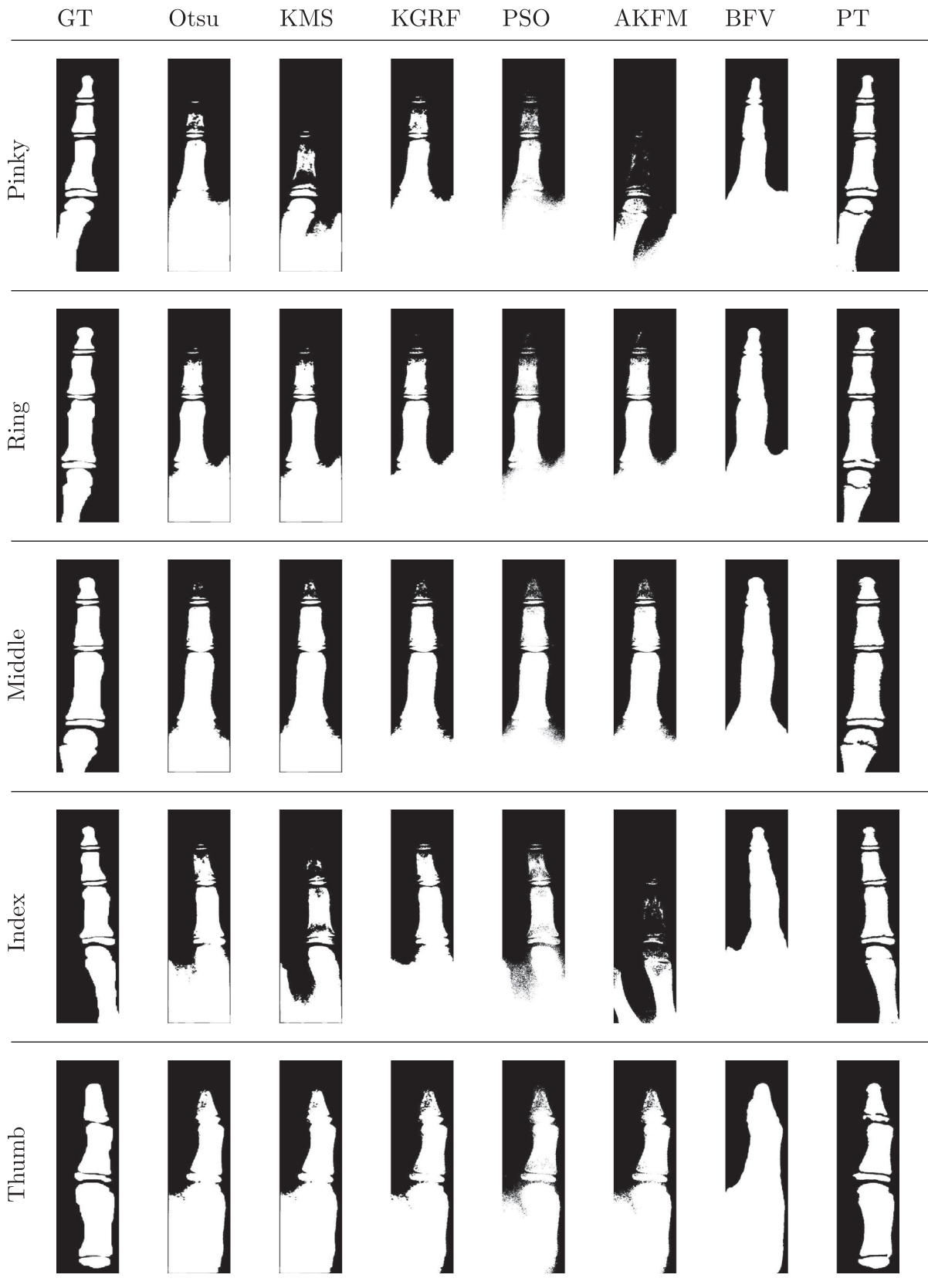


Figure 11. Segmentation results of different algorithms on hand radiograph taken from 9 year old person [5125.jpg].

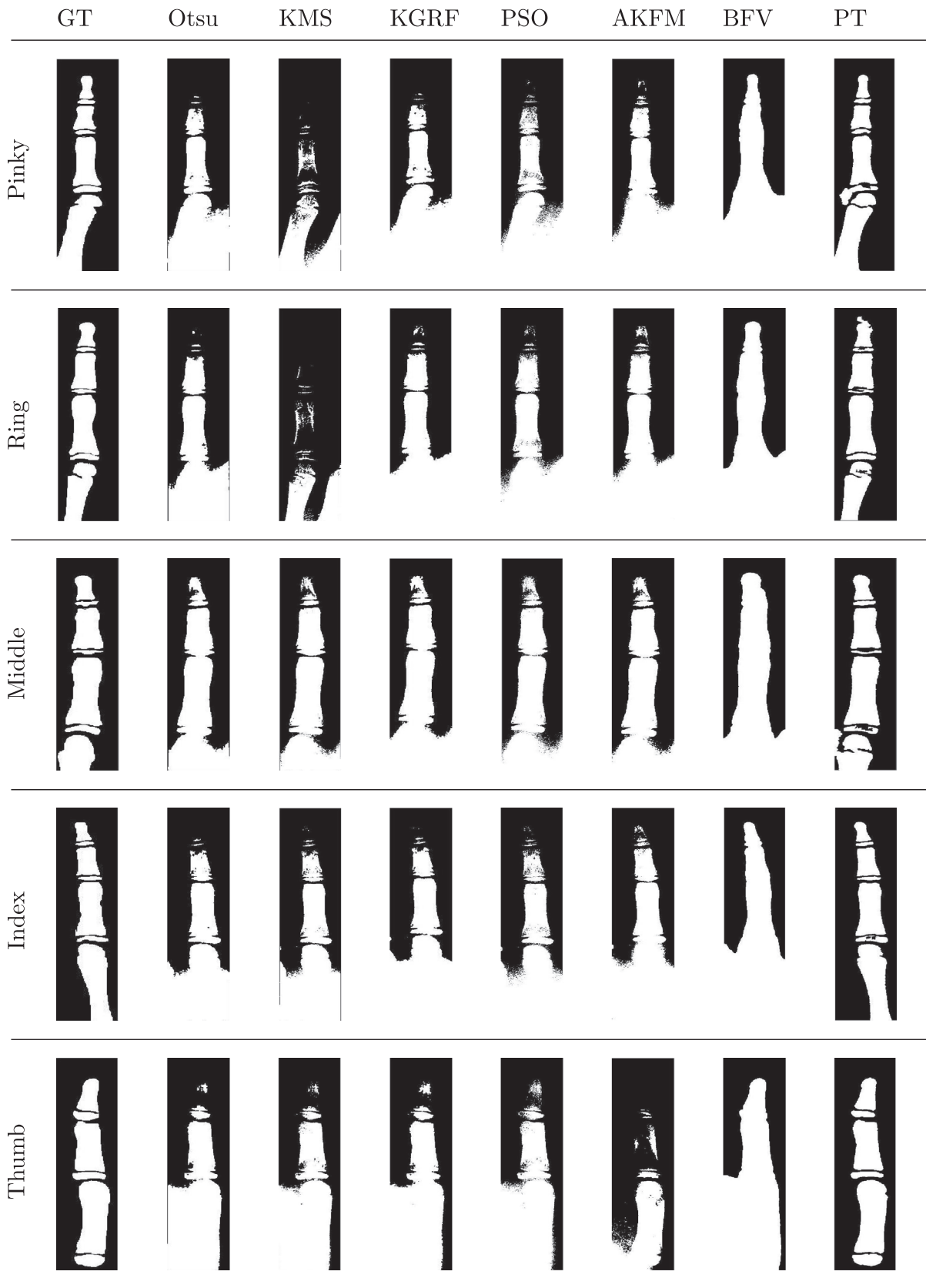


Figure 12. Segmentation results of different algorithms on hand radiograph taken from 10 year old person [5113.jpg].

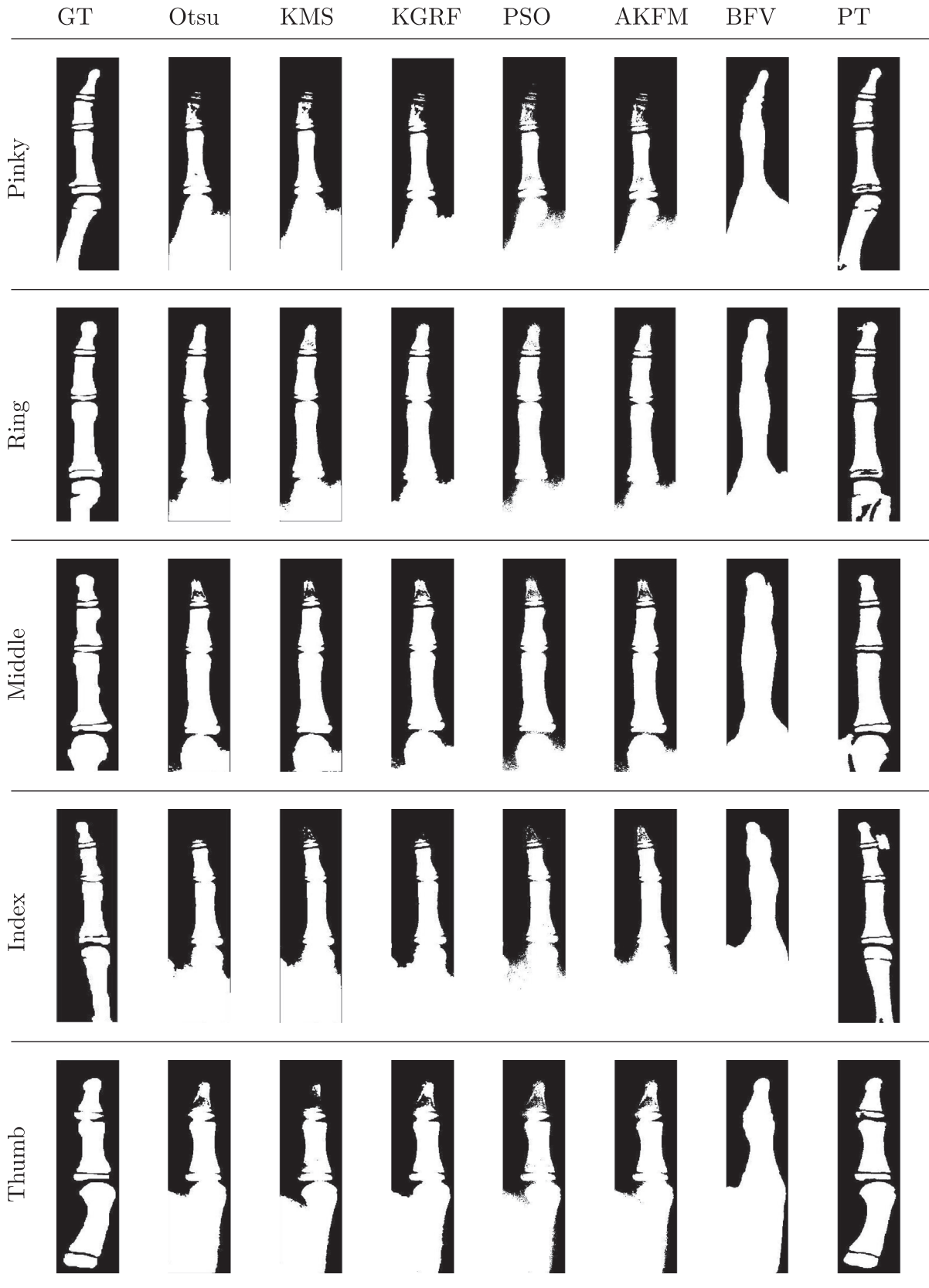


Figure 13. Segmentation results of different algorithms on hand radiograph taken from 12 year old person [5322.jpg].

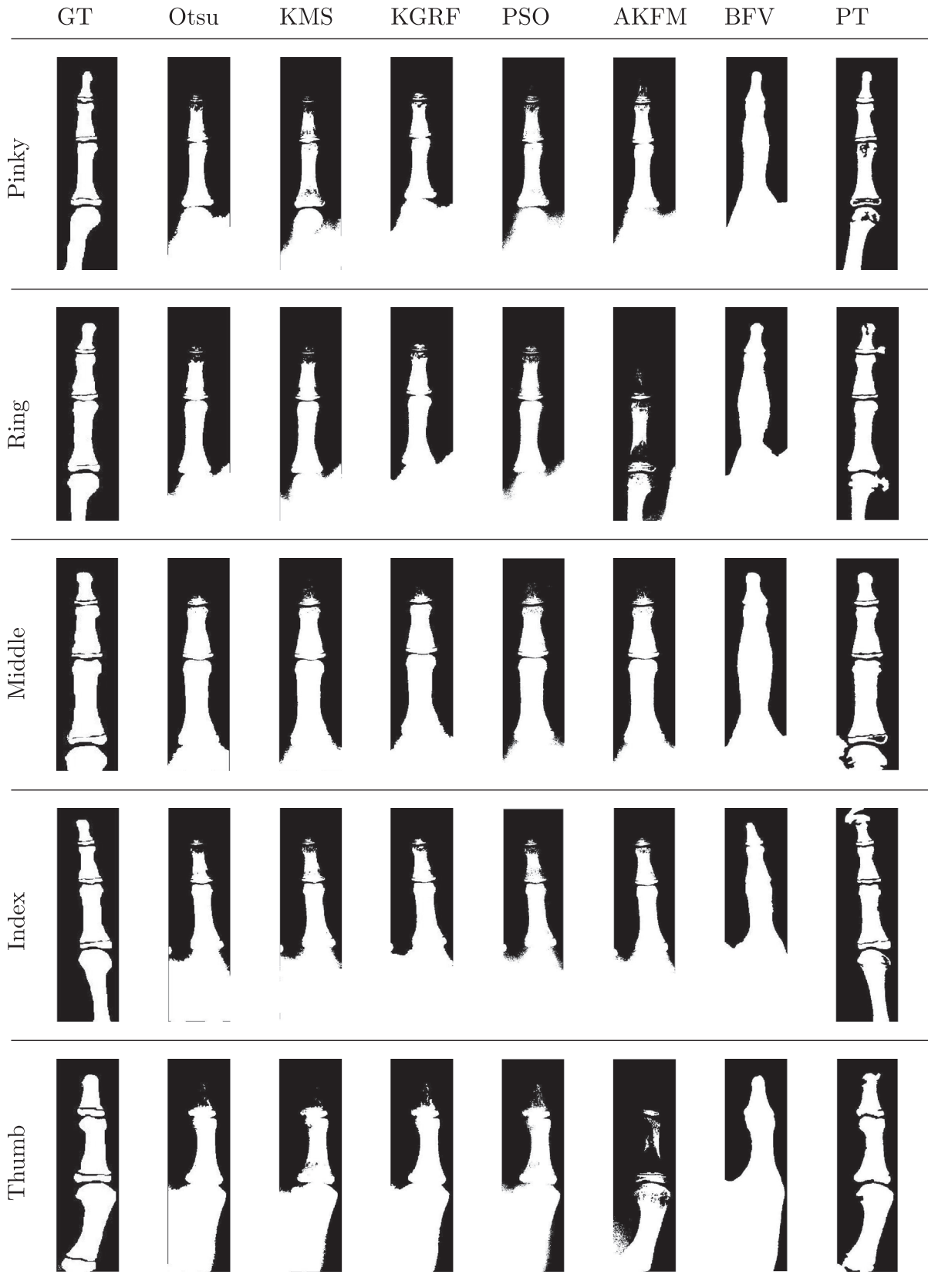


Figure 14. Segmentation results of different algorithms on hand radiograph taken from 14 year old person [5237.jpg].



Figure 15. Segmentation results of different algorithms on hand radiograph taken from 16 year old person [5257.jpg].

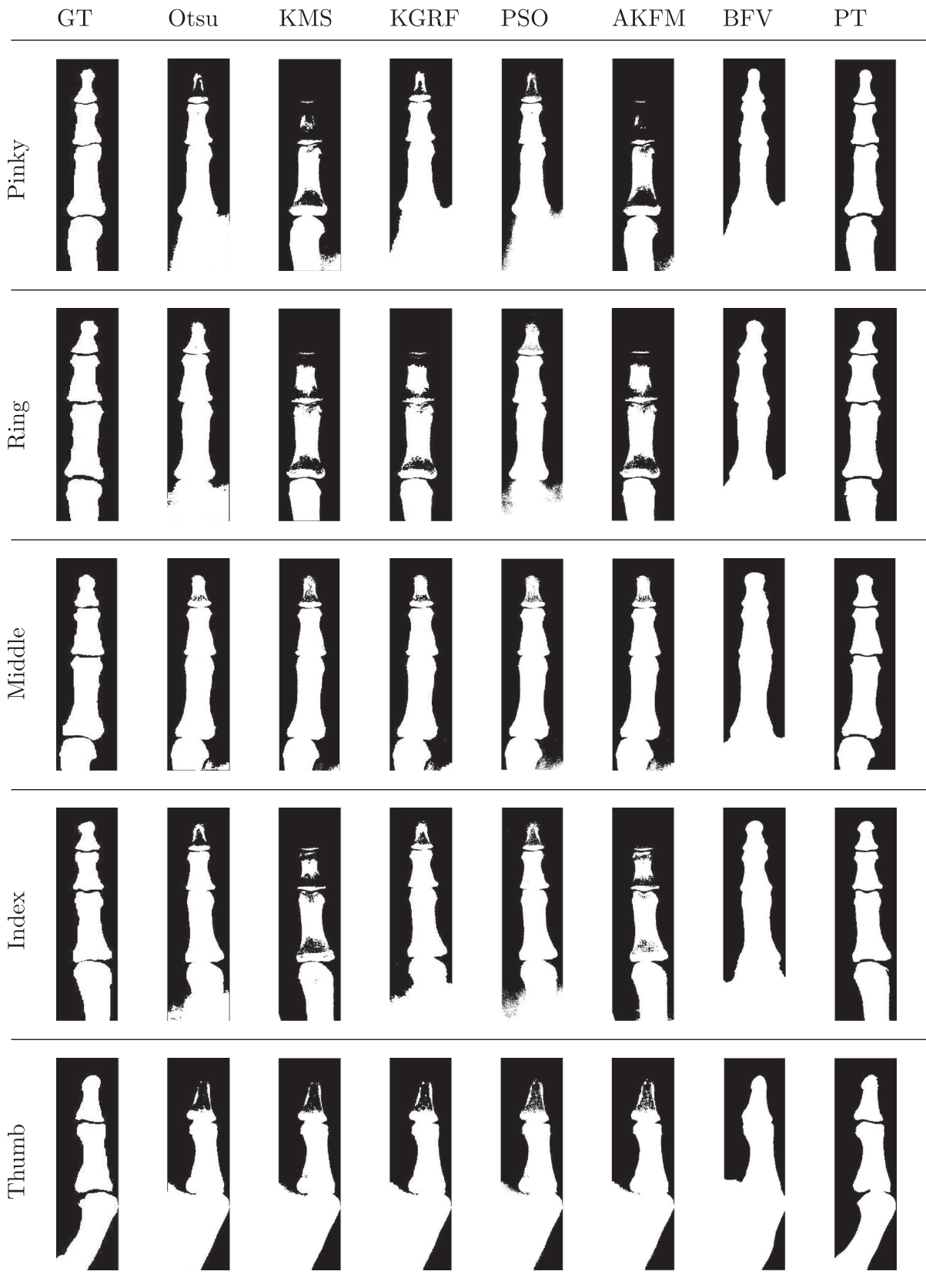


Figure 16. Segmentation results of different algorithms on hand radiograph taken from 18 year old person [6145.jpg].

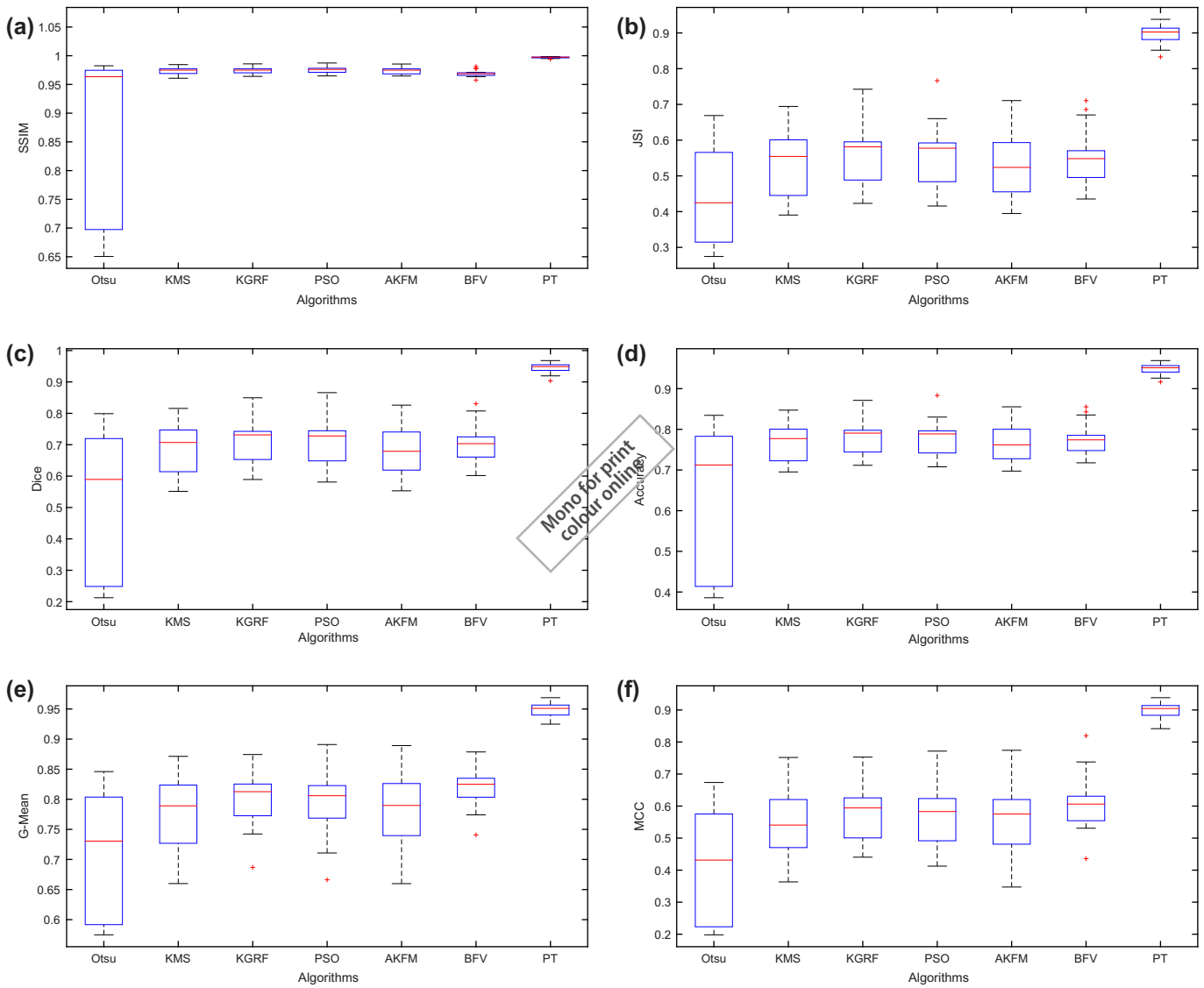


Figure 17. Boxplots of segmentation techniques against various quality metrics for PROI.

4.2. Performance metrics

The quantitative and qualitative results of proposed segmentation technique (PT) and other state-of-the-art segmentation techniques such as Otsu's thresholding by Otsu (1979), KMS by Hartigan and Wong (1979), KGRF by Pappas and Jayant (1988), PSO based segmentation algorithm (PSO) by Eberhart and Kennedy (1995), AKFM by Elazab et al. (2015) and BFV algorithm (BFV) by Gong et al. (2015) are evaluated on digital hand radiographs and presented in this section. To evaluate the performance of proposed technique (PT), improvement at each stage is checked using quality metrics like PSNR, MSE and SSIM which are given in Equations (22), (21) and (23), respectively. To judge the robustness of proposed technique with other state-of-the-art segmentation techniques mentioned earlier, we use various quality metrics such as Structure similarity index (SSIM), Jaccard Similarity Index (JSI), Dice, Accuracy (ACC), Geometric Mean (GM) and Matthews Correlation Coefficient (MCC) are the automatic choice for the researchers in the field of medical image segmentation. The mathematical expressions for PSNR and MSE are as follows:

$$MSE = \frac{1}{MN} \sum_{i=1}^M \sum_{j=1}^N (S - G)^2 \quad (21)$$

where S stands for segmented image and G for ground truth image.

$$PSNR(dB) = 10 * \log_{10} \left(\frac{255^2}{MSE} \right) \quad (22)$$

SSIM is given by equation:

$$SSIM(S, G) = \frac{(2\mu_S\mu_G + \lambda_1)(2\sigma_{SG} + \lambda_2)}{(\mu_S^2 + \mu_G^2 + \lambda_1)(\sigma_S^2 + \sigma_G^2 + \lambda_2)} \quad (23)$$

μ_S, σ_S are the mean and variance of segmented image and μ_G, σ_G are the mean and variance of ground truth image. σ_{SG} is the covariance and λ_1, λ_2 are small constants to stabilise the denominator. The numerical value of SSIM lies between 0 and 1. The proximity of SSIM value closer to 1, better is the segmentation technique.

Table 1. PSNR, MSE, SSIM performance comparison of results after each stage of the proposed technique on hand radiographs of ages 1, 5, 10, 12 and 16-year old person.

Image	PROI	QM	Edge preservation	Segmentation	Post-processing
1 year, [5173.jpg]	Pinky	PSNR	19.977	45.592	65.079
		MSE	653.660	1.794	0.020
		SSIM	0.914	0.812	0.999
	Ring	PSNR	19.117	45.840	65.142
		MSE	796.786	1.695	0.020
		SSIM	0.907	0.825	0.999
	Middle	PSNR	19.830	47.787	61.864
		MSE	676.210	1.082	0.042
		SSIM	0.897	0.880	0.996
	Index	PSNR	21.807	45.944	64.269
		MSE	428.892	1.655	0.024
		SSIM	0.943	0.831	0.998
	Thumb	PSNR	20.772	47.787	65.115
		MSE	544.356	1.082	0.020
		SSIM	0.933	0.875	0.999
5 year, [7143.jpg]	Pinky	PSNR	18.901	47.235	64.306
		MSE	837.579	1.229	0.024
		SSIM	0.931	0.864	0.998
	Ring	PSNR	20.112	47.384	62.571
		MSE	633.642	1.188	0.036
		SSIM	0.939	0.870	0.997
	Middle	PSNR	19.311	46.583	58.957
		MSE	762.000	1.428	0.083
		SSIM	0.940	0.852	0.991
	Index	PSNR	20.006	46.780	62.516
		MSE	649.314	1.365	0.036
		SSIM	0.946	0.854	0.997
	Thumb	PSNR	20.780	46.148	63.495
		MSE	543.346	1.579	0.029
		SSIM	0.936	0.838	0.997
10 year, [5113.jpg]	Pinky	PSNR	19.085	46.240	62.606
		MSE	802.816	1.546	0.036
		SSIM	0.848	0.838	0.997
	Ring	PSNR	24.133	46.730	63.070
		MSE	251.062	1.381	0.032
		SSIM	0.849	0.855	0.997
	Middle	PSNR	23.000	46.904	61.824
		MSE	325.894	1.326	0.043
		SSIM	0.869	0.860	0.997
	Index	PSNR	25.790	46.403	64.823
		MSE	171.436	1.489	0.021
		SSIM	0.864	0.845	0.998
	Thumb	PSNR	21.172	46.470	64.218
		MSE	496.485	1.466	0.025
		SSIM	0.861	0.849	0.998
12 year, [5322.jpg]	Pinky	PSNR	21.281	46.364	63.123
		MSE	484.132	1.502	0.032
		SSIM	0.981	0.839	0.997
	Ring	PSNR	25.696	46.517	59.749
		MSE	175.160	1.450	0.069
		SSIM	0.986	0.847	0.993
	Middle	PSNR	24.497	46.557	59.367
		MSE	230.855	1.437	0.075
		SSIM	0.987	0.850	0.992
	Index	PSNR	28.104	46.319	62.066
		MSE	100.612	1.518	0.040
		SSIM	0.991	0.840	0.996
	Thumb	PSNR	27.765	46.476	63.033
		MSE	108.782	1.464	0.032
		SSIM	0.981	0.848	0.997
16 years, [5257.jpg]	Pinky	PSNR	21.16	47.088	62.601
		MSE	497.145	1.272	0.036
		SSIM	0.887	0.877	0.997
	Ring	PSNR	22.573	47.537	61.874
		MSE	359.611	1.147	0.042
		SSIM	0.919	0.877	0.996
	Middle	PSNR	20.563	47.663	61.835
		MSE	571.167	1.114	0.043
		SSIM	0.973	0.880	0.996

(Continued)

Table 1. (Continued).

Image	PROI	QM	Edge preservation	Segmentation	Post-processing
		PSNR	24.310	46.969	63.972
	Index	MSE	241.055	1.307	0.026
		SSIM	0.956	0.859	0.998
		PSNR	21.657	47.133	60.181
	Thumb	MSE	444.010	1.258	0.062
		SSIM	0.905	0.868	0.994

Table 2. Simulation parameters and their values used by various techniques.

Parameters	Otsu	KMS	KGRF	PSO	AKFM	BFV	PT
Number of thresholds	2						
Number of clusters		3	3	3	3		
Number of iterations			30	150		200	100
Clique potential			0.5				
Local filtering					median	gaussian	gaussian
Local window size					3	10	3
Population				150			
Inertial weight				1.2			
Weight 1				0.8		1	
Weight 2				0.8		1	
Min velocity				-5			
Max velocity				5			
Lower bound of position				1			
Upper bound of position				256			
Constant positive integer						2	
Time step						0.1	0.1
Heavyside weight							1

JSI and Dice similarity as mentioned by [Simu and Lal \(2017\)](#) is used for performance analysis:

$$JSI = \frac{|S \cap G|}{|S \cup G|} \quad (24)$$

$$Dice = 2 \frac{|S \cap G|}{|S + G|} \quad (25)$$

Dice coefficient is also called as the F1 score. Jaccard coefficient and Dice coefficient look similar but they are not same. Both are used to measure the similarity index but Dice does not satisfy the triangle inequality. The numerical values of both coefficients lie between 0 and 1. The proximity of JSI and Dice values closer to 1, better is the segmentation technique.

Accuracy (ACC) as used by [Simu and Lal \(2017\)](#) gives information about the ratio of the pixels contained within the segmented region achieved by the test algorithm with the pixels of the manually segmented region. The segmentation accuracy is defined as,

$$ACC = \frac{t_p + t_n}{t_p + f_p + t_n + f_n} \quad (26)$$

where t_p = true positive, t_n = true negative, f_p = false positive and f_n = false negative. The numerical value of ACC lies between 0 and 1, where 0 corresponds to failed segmentation and 1 corresponds to best segmentation accuracy.

The geometric mean (GM) given by [Orlando et al. \(2017\)](#) is calculated as:

$$GM = \sqrt{\frac{t_p t_n}{(t_p + f_n)(t_n + f_p)}} \quad (27)$$

The numerical value of GM lies between 0 and 1. The proximity of GM value closer to 1, better is the segmentation technique.

The mathematical equation for MCC as used by [Orlando et al. \(2017\)](#) is given as:

$$MCC = \frac{(t_p t_n) - (f_p f_n)}{\sqrt{(t_p + f_p)(t_p + f_n)(t_n + f_p)(t_n + f_n)}} \quad (28)$$

MCC is considered as a balanced measure as it can be used also when the classes vary in sizes. The MCC value varies between -1 and +1. Where +1 means a perfect segmentation and -1 indicates complete fallout between segmented and ground truth images.

4.3. Segmentation results

The hand radiograph is divided into three regions namely background, the soft tissue region and the bones. Hence the parameter values of segmentation techniques used are set accordingly. Otsu's thresholding is done using two levels to separate the three regions while other techniques like KMS, KGRF and PSO-based segmentation algorithm (PSO) have a number of classes set to three for segmentation. Table 2 shows the parameters used for simulation of these segmentation techniques and their values. The first four techniques namely Otsu, KMS, KGRF and PSO have been implemented in the field of hand bone segmentation earlier by [Kashif et al. \(2015\)](#), [Pietka et al. \(2003\)](#), [Trist-Vega and Arribas \(2008\)](#) and [Liu et al. \(2007\)](#), respectively. AKFM is a recent fuzzy based clustering algorithm which was implemented on brain tissues by [Elazab et al. \(2015\)](#), has been included for comparison. BFV algorithm (BFV) developed by [Gong et al. \(2015\)](#) is a recent fuzzy based level set algorithm, which is also included for comparison. Please note that all hand radiographs used for comparison have also been subjected to anisotropic diffusion as pre-processing step before application

Table 3. Performance comparison of different segmentation techniques on PROI.

Image	QM	Otsu	KMS	KGRF	PSO	AKFM	BFV	PT
1 year [5173.jpg]	SSIM	0.650	0.965	0.966	0.967	0.967	0.965	0.998
	JSI	0.274	0.468	0.462	0.461	0.415	0.491	0.912
	DICE	0.213	0.634	0.629	0.628	0.580	0.655	0.954
	ACC	0.386	0.734	0.731	0.731	0.708	0.745	0.956
	GM	0.575	0.760	0.767	0.764	0.767	0.801	0.955
	MCC	0.198	0.475	0.483	0.478	0.482	0.547	0.913
3 years [6102.jpg]	SSIM	0.681	0.978	0.977	0.977	0.978	0.970	0.994
	JSI	0.287	0.603	0.595	0.593	0.595	0.549	0.833
	DICE	0.231	0.748	0.741	0.740	0.741	0.703	0.904
	ACC	0.403	0.802	0.798	0.796	0.798	0.774	0.916
	GM	0.586	0.832	0.832	0.831	0.831	0.828	0.925
	MCC	0.212	0.630	0.629	0.626	0.632	0.606	0.842
5 years [7143.jpg]	SSIM	0.676	0.969	0.969	0.970	0.968	0.969	0.996
	JSI	0.317	0.436	0.529	0.525	0.417	0.548	0.881
	DICE	0.245	0.594	0.690	0.686	0.569	0.706	0.936
	ACC	0.403	0.718	0.764	0.762	0.709	0.774	0.941
	GM	0.582	0.660	0.791	0.784	0.672	0.774	0.941
	MCC	0.217	0.375	0.543	0.532	0.406	0.820	0.882
7 years [5154.jpg]	SSIM	0.673	0.975	0.975	0.975	0.975	0.966	0.998
	JSI	0.315	0.592	0.588	0.586	0.588	0.536	0.912
	DICE	0.243	0.741	0.738	0.746	0.738	0.697	0.954
	ACC	0.401	0.796	0.794	0.793	0.794	0.768	0.956
	GM	0.581	0.824	0.826	0.825	0.827	0.825	0.957
	MCC	0.216	0.615	0.618	0.615	0.618	0.600	0.913
9 years [5125.jpg]	SSIM	0.973	0.974	0.973	0.975	0.973	0.970	0.997
	JSI	0.574	0.554	0.574	0.569	0.497	0.572	0.903
	DICE	0.726	0.707	0.726	0.722	0.649	0.726	0.949
	ACC	0.787	0.777	0.787	0.784	0.749	0.786	0.951
	GM	0.804	0.777	0.810	0.801	0.726	0.835	0.950
	MCC	0.579	0.541	0.587	0.573	0.481	0.629	0.905
10 years [7076.jpg]	SSIM	0.700	0.975	0.977	0.977	0.976	0.971	0.997
	JSI	0.314	0.506	0.595	0.590	0.575	0.575	0.901
	DICE	0.253	0.653	0.743	0.739	0.725	0.728	0.948
	ACC	0.415	0.753	0.798	0.795	0.788	0.788	0.951
	GM	0.592	0.747	0.817	0.812	0.824	0.837	0.951
	MCC	0.226	0.512	0.606	0.596	0.617	0.632	0.904
12 years [5322.jpg]	SSIM	0.697	0.978	0.978	0.979	0.978	0.968	0.995
	JSI	0.309	0.617	0.615	0.615	0.616	0.549	0.852
	DICE	0.249	0.758	0.757	0.757	0.757	0.707	0.919
	ACC	0.413	0.809	0.808	0.808	0.808	0.775	0.926
	GM	0.591	0.822	0.828	0.827	0.823	0.830	0.925
	MCC	0.223	0.622	0.628	0.628	0.621	0.614	0.851
14 years [5237.jpg]	SSIM	0.705	0.976	0.976	0.976	0.976	0.971	0.996
	JSI	0.302	0.575	0.581	0.577	0.524	0.563	0.858
	DICE	0.248	0.726	0.731	0.728	0.679	0.717	0.924
	ACC	0.417	0.787	0.791	0.789	0.762	0.782	0.929
	GM	0.595	0.748	0.813	0.806	0.791	0.832	0.928
	MCC	0.224	0.506	0.594	0.583	0.575	0.620	0.859
16 years [5257.jpg]	SSIM	0.804	0.969	0.973	0.972	0.975	0.978	0.996
	JSI	0.370	0.413	0.475	0.446	0.586	0.671	0.893
	DICE	0.347	0.575	0.632	0.610	0.728	0.800	0.943
	ACC	0.496	0.706	0.738	0.723	0.793	0.835	0.946
	GM	0.647	0.676	0.687	0.666	0.790	0.861	0.946
	MCC	0.296	0.469	0.483	0.463	0.597	0.697	0.893
18 years [6145.jpg]	SSIM	0.714	0.985	0.986	0.987	0.986	0.981	0.998
	JSI	0.379	0.694	0.742	0.766	0.711	0.706	0.938
	DICE	0.294	0.816	0.850	0.866	0.826	0.828	0.968
	ACC	0.431	0.847	0.871	0.883	0.855	0.853	0.969
	GM	0.596	0.871	0.874	0.891	0.889	0.879	0.969
	MCC	0.247	0.752	0.753	0.772	0.774	0.738	0.938

of the various segmentation techniques for fair comparison with PT.

The quantitative performance analysis of proposed fully automatic segmentation technique and other state-of-the-art techniques are obtained for PROI images at ages 1 [5173.jpg], 3 [6102.jpg], 5 [7143.jpg], 7 [5154.jpg], 9 [5125.jpg], 10 [5113.jpg], 12 [5322.jpg], 14 [5237.jpg], 16 [5257.jpg] and 18 [6145.jpg] are given in Table 3. The results of additional 9 images are added

in the supplementary materials. In Table 3 the results shown are the average values of all 5 fingers i.e. pinky, ring, middle, index and thumb. From Table 3 it is clear that proposed segmentation technique achieved better quantitative metrics such as SSIM, JSI, Dice, ACC, GM and MCC as compared to other state-of-the-art techniques.

The qualitative results of proposed fully automatic segmentation technique and other state-of-the-art techniques are given

Table 4. Statistical values of various quality metrics against segmentation techniques.

QM	Statistic	Otsu	KMS	KGRF	PSO	AKFM	BFV	PT
SSIM	MIN	0.650	0.961	0.964	0.965	0.965	0.958	0.994
	MAX	0.983	0.985	0.986	0.987	0.986	0.981	0.999
	MEAN	0.844	0.974	0.974	0.975	0.974	0.969	0.997
	MEDIAN	0.964	0.975	0.975	0.976	0.975	0.969	0.997
	SDEV	0.139	0.006	0.005	0.005	0.005	0.005	0.001
JSI	MIN	0.274	0.390	0.423	0.416	0.395	0.435	0.833
	MAX	0.669	0.694	0.742	0.766	0.711	0.711	0.938
	MEAN	0.440	0.540	0.561	0.556	0.532	0.548	0.895
	MEDIAN	0.425	0.554	0.581	0.577	0.524	0.548	0.903
	SDEV	0.130	0.091	0.079	0.085	0.087	0.073	0.026
DICE	MIN	0.213	0.551	0.589	0.581	0.553	0.602	0.904
	MAX	0.799	0.816	0.850	0.866	0.826	0.830	0.968
	MEAN	0.492	0.691	0.711	0.708	0.683	0.703	0.944
	MEDIAN	0.589	0.707	0.731	0.728	0.679	0.703	0.949
	SDEV	0.228	0.080	0.065	0.071	0.077	0.060	0.015
ACC	MIN	0.386	0.695	0.712	0.708	0.697	0.718	0.916
	MAX	0.834	0.847	0.871	0.883	0.855	0.855	0.969
	MEAN	0.606	0.770	0.780	0.778	0.767	0.774	0.948
	MEDIAN	0.712	0.777	0.791	0.789	0.762	0.774	0.951
	SDEV	0.181	0.045	0.039	0.043	0.044	0.037	0.013
GM	MIN	0.575	0.660	0.687	0.666	0.660	0.741	0.925
	MAX	0.846	0.871	0.874	0.891	0.889	0.879	0.969
	MEAN	0.699	0.775	0.800	0.794	0.780	0.822	0.947
	MEDIAN	0.731	0.789	0.813	0.806	0.790	0.825	0.951
	SDEV	0.104	0.061	0.041	0.049	0.057	0.031	0.012
MCC	MIN	0.198	0.363	0.440	0.412	0.347	0.436	0.842
	MAX	0.674	0.752	0.753	0.772	0.774	0.820	0.938
	MEAN	0.401	0.544	0.576	0.567	0.549	0.614	0.897
	MEDIAN	0.431	0.541	0.594	0.583	0.575	0.606	0.905
	SDEV	0.174	0.105	0.078	0.087	0.103	0.082	0.025

Note: The bold values represent best results.

Table 5. Computation time required for each of the segmentation techniques (seconds).

Images	Otsu	KMS	KGRF	PSO	AKFM	BFV	PT
1 year [5173.jpg]	0.542	0.567	0.702	2.315	4.416	1.667	9.479
3 years [6102.jpg]	0.576	1.563	0.956	4.116	9.632	3.047	33.406
5 years [7143.jpg]	0.597	0.618	1.077	2.438	6.338	2.237	35.652
7 years [5154.jpg]	0.614	0.962	1.337	4.406	12.962	3.938	31.100
9 years [5125.jpg]	0.594	0.719	1.367	2.567	9.543	3.418	33.749
10 years [5133.jpg]	0.643	1.089	1.622	4.636	16.187	4.704	31.250
12 years [5322.jpg]	0.736	0.831	1.717	2.733	11.791	4.313	47.967
14 years [5237.jpg]	0.950	1.420	2.594	5.033	27.104	7.451	70.572
16 years [5257.jpg]	0.742	0.877	2.092	2.809	13.374	4.952	55.022
18 years [6145.jpg]	0.743	1.324	2.128	4.840	24.629	6.781	84.590

in Figures 7–16 for ages 1, 3, 5, 7, 9, 10, 12, 14, 16 and 18, respectively. Ground truth images (GT) have also been included for comparison in Figures 7–16. The qualitative results of other images are provided in supplementary materials in Figures S.5 to S.13 for ages under 1, 2, 4, 6, 8, 11, 13, 15 and 17, respectively.

Box-plot has been used to compare all the segmentation techniques with respect to various quality metrics and is shown in Figure 17, wherein the sample size is 10 (number of images). The interquartile range (IQR) is denoted by box and whiskers denoted by line with breaks defines the range. The whisker length is increased to engulf outliers into the range of data. The median is denoted by a line in the IQR which is skewed in some cases due to the sample being skewed positively or negatively.

From the box-plot shown in Figure 17, it can be noticed that proposed segmentation technique has less variation compared to other techniques and also achieves higher segmentation accuracy in terms of all the quality metrics. The SSIM

boxplot against various techniques shown in Figure 17(a) indicates that Otsu's thresholding performs poorly compared to other techniques. The SSIM values of other techniques are above 0.95 but proposed technique has values around 0.99. The boxplot of JSI shown in Figure 17(b) shows proposed technique takes the value around 0.9 and supersedes other state-of-the-art techniques. Similarly in all other boxplots i.e. Figures 17(c)–(f) the proposed technique has higher quality metric values against other state-of-the-art techniques (approximately 0.95). The visual comparison of segmentation results of proposed technique and other state-of-the-art segmentation techniques are given from Figures 7–16. It can be noticed from Figures 7–17 and Figures S.5 to S.13 from the supplementary materials, that proposed segmentation technique (PT) gives better segmentation results as compared to other state-of-the-art techniques. In Table 4, statistical values such as minimum (MIN), maximum (MAX), mean, median and standard deviation (SDEV) of various quality metrics against segmentation techniques have been presented.

Table 6. Ratings given by medical experts to the segmentation results of PROI for our proposed technique.

Age (years)	Finger	Expert-1	Expert-2	Expert-3	Expert-4	Average Rating	Overall average
01	Pinky	5	5	5	5	5	4.4
	Ring	5	5	5	5	5	
	Middle	3	4	3	4	3.5	
	Index	3	4	4	3	3.5	
	Thumb	5	5	5	5	5	
03	Pinky	3	3	4	3	3.25	4.4
	Ring	4	3	4	4	3.75	
	Middle	5	5	5	5	5	
	Index	5	5	5	5	5	
	Thumb	5	5	5	5	5	
05	Pinky	4	4	4	4	4	3.3
	Ring	4	4	4	4	4	
	Middle	3	3	3	3	3	
	Index	2	3	3	3	2.75	
	Thumb	2	3	3	3	2.75	
07	Pinky	5	5	5	5	5	4.45
	Ring	4	5	5	5	4.75	
	Middle	5	3	4	4	4	
	Index	4	3	4	3	3.5	
	Thumb	5	5	5	5	5	
09	Pinky	4	4	5	5	4.5	4.7
	Ring	4	4	5	5	4.5	
	Middle	4	4	5	5	4.5	
	Index	5	5	5	5	5	
	Thumb	5	5	5	5	5	
10	Pinky	5	2	4	3	3.5	4.25
	Ring	4	4	4	4	4	
	Middle	4	4	4	5	4.25	
	Index	5	4	5	4	4.5	
	Thumb	5	5	5	5	5	
12	Pinky	3	4	4	3	3.5	3.6
	Ring	3	3	3	4	3.25	
	Middle	3	4	4	3	3.5	
	Index	3	3	3	4	3.25	
	Thumb	4	4	5	5	4.5	
14	Pinky	3	3	4	3	3.25	3.85
	Ring	2	3	4	4	3.25	
	Middle	5	4	5	4	4.5	
	Index	4	4	5	4	4.25	
	Thumb	2	4	5	5	4	
16	Pinky	4	4	4	4	4	4.45
	Ring	4	4	5	5	4.5	
	Middle	4	4	4	4	4	
	Index	5	5	5	5	5	
	Thumb	5	4	5	5	4.75	
18	Pinky	5	5	5	5	5	5
	Ring	5	5	5	5	5	
	Middle	5	5	5	5	5	
	Index	5	5	5	5	5	
	Thumb	5	5	5	5	5	

4.4. Computational cost

The time taken by various segmentation techniques are presented in the Table 5. The computational time recorded in the table is average time of five PROI's of each hand radiograph. The time calculated is total time taken by anisotropic diffusion and segmentation technique. Anisotropic diffusion has been used as pre-processing technique on PROI's for all segmentation techniques compared. From the Table 5, we can see that computational cost of proposed technique is more as compared to other state-of-the-art segmentation techniques. The computational cost for proposed technique is two to three times more than ARKFCM technique, but roughly takes 10 times more time than other segmentation techniques. Even if the time taken by proposed technique is more compared to other techniques it supersedes them with respect to the segmentation accuracy that

is achieved. In ABAA, for further analysis which includes feature extraction and classification stages, a higher segmentation accuracy is of utmost importance.

4.5. Segmentation accuracy

The quality metrics JSI, Dice, ACC and MCC give vital information about the segmentation accuracy of proposed fully automatic segmentation technique. From the quantitative analysis as given in the Table 6 we can see that the proposed technique performs far better than other segmentation techniques. The ratings given by different medical experts are given in the Table 6. Each of the segmented results obtained using proposed technique has been rated between 1–5 with value 1 being very poor, 2 – poor, 3 – average, 4 – good, 5 – excellent. The medical experts have com-

pared the segmented image obtained using proposed technique with ground truth image and original hand radiograph image visually and given the ratings. In Table 6, we can see that medical experts have rated 4 or 5 to the segmentation results indicating that the outcome is fair enough. In cases where the values are 3 or below the proposed technique has not been accurate enough. The reason for this is the low radiation intensity used for children at a younger age as given in Behiels et al. (2001).

4.6. Major findings

The major findings of this research work are as follows:

- (1) Proposed fully automatic PROI extraction method for phalanges from hand radiographs is simple, fast, accurate and it extracts all 5 phalangeal regions at the same time.
- (2) Proposed fully automatic segmentation technique has been able to tackle the heel effect problem or the intensity inhomogeneity due to bias field that was present in the hand radiograph.
- (3) Proposed segmentation technique has been able to provide very good quantitative and qualitative segmentation results, but it takes a little more processing time as compared to other existing segmentation techniques.

5. Conclusion

The proposed fully automatic technique presented in this paper has been very effective and robust for segmentation of phalanges from hand radiographs. All techniques used for comparison including the proposed technique have been validated on database as mentioned previously with an age group of 0–18 years. The database included under-exposed as well as over-exposed radiographic images. The proposed segmentation technique provided an approximate segmentation accuracy of 94%. The mean values of various quality metrics used like SSIM, JSI, Dice, ACC, GM and MCC are 0.997, 0.895, 0.944, 0.948, 0.947 and 0.897, respectively.

The proposed fully automatic ROI extraction developed was fast and accurate with no extraction error. The automatic ROI extraction was independent of hand placement and orientation. Also, it is simple and takes a negligible amount of time. Experimental results demonstrated that proposed segmentation technique provided better quantitative and qualitative results as compared to other existing segmentation techniques. The segmentation results have been also verified by different medical experts. The overall average rating given by all the medical experts are above the average value of 3. Advantages of proposed technique were that it was very effective and robust. Few errors in the segmentation using proposed technique persist, which we aim to tackle in the feature extraction stage. The medical experts have given a lower rating to these segmentation results which are radiographs of young people. The hand radiographs of young people were obtained with exposure to less radiation due to medical norms, hence the clarity of the image is affected. Another drawback of proposed technique is that computational cost required is more among all compared techniques. But in the field of medical image processing and analysis time taken around a minute is negligible concern and utmost importance is given to the accuracy of results which we have achieved. In TW3

assessment 3 fingers and radius-ulna bones are used for evaluating the bone age. We aim to use all five fingers for achieving higher accuracy. Nevertheless, the proposed technique being robust can be applied for automated bone age assessment of a person whose age is unknown.

The future work in automated bone age assessment procedure is designing an effective feature extraction and robust classification technique, by which we can negate the errors of segmentation such that it does not affect the overall bone score and give a very precise estimation of age.

Acknowledgements

The authors would like to thank the editor and anonymous reviewers for their constructive comments, which improved the quality of the manuscript. The authors would also like to thank Dr. Pranav Nagarsenkar from Goa Medical College, Goa, India and Dr. Amresh Naik from Directorate of Health Services, Panjim, Goa, India for helping with creation of ground truth images, validating the segmentation results and reviewing the manuscript. Special thanks to Professor Roberto A. Lotufo from the University of Campinas for helping out with the license of morphology toolbox, which has been an immense help.

Disclosure statement

No potential conflict of interest was reported by the authors.

Notes on contributors

Shreyas Simu received MTech degree in Digital Electronics and Advance Communication from Manipal University, Manipal, India, in 2012 and is currently working towards the PhD degree in medical image processing from National Institute of Technology, Karnataka, India. His research interests include image processing and machine learning.

Shyam Lal received the MTech degree in Electronics and Communication engineering from NIT Kurukshetra, Kurukshetra, India, in 2007, and the PhD degree in image processing from BIT Mesra, Ranchi, India, in 2013. He has been working as an assistant professor in the Department of Electronics & Communication Engineering, National Institute of Technology Karnataka, Mangalore, India. His research interests include digital image processing, remote sensing, and medical image processing.

Kunal Fadte received MBBS degree from Goa University, Goa, India in 2011 and MS degree in orthopedic surgery from Goa University in 2016. He is currently working as Senior Resident at Goa Medical College, Bambolim, Goa, India. His interest includes joint surgery.

Atteeque Harlapur is currently working as tutor in Department of Biochemistry at Belgaum Institute of Medical Sciences, Belgavi, India.

ORCID

Shreyas Simu  <http://orcid.org/0000-0002-1004-3974>

References

- Behiels G, Maes F, Vandermeulen D, Suetens P. 2001. Retrospective heel effect correction in conventional radiography. In: IEEE Workshop on Mathematical Methods in Biomedical Image Analysis, 2001. MMBIA 2001. Dec 9–10; Kauai, HI; p. 87–94.
- Census of India-2011. 2011. New Delhi: registrar general and census commissioner of India. <http://censusindia.gov.in/>.
- Chai HY, Swee TT, Seng GH, Wee LK. 2013. Multipurpose contrast enhancement on epiphyseal plates and ossification centers for bone age assessment. Biomed Eng. 12(1):1–19. online.

- Chai HY, Wee LK, Swee TT, Hussain S. 2011. Glcm based adaptive crossed reconstructed (acr) k-mean clustering hand bone segmentation. In: Proceeding of 10th WSEAS International Conference on Electronics, Hardware, Wireless and Optical Communications, and 10th WSEAS International Conference on Signal Processing, Robotics and Automation, and 3rd WSEAS International Conference on Nanotechnology, and 2Nd WSEAS International Conference on Plasma-fusion-nuclear Physics; Stevens Point, Wisconsin, USA, NEHIPISIC'11. World Scientific and Engineering Academy and Society (WSEAS). <http://dl.acm.org/citation.cfm?id=1959586.1959625>.
- Chan TF, Vese LA. 2001. Active contours without edges. *IEEE Trans Image Process.* 10(2):266–277.
- Dougherty ER, Lotufo RA. 2003. Hands-on morphological image processing. Vol. 71, Washington: SPIE Optical Engineering Press.
- Eberhart RC, Kennedy J, et al. 1995. A new optimiser using particle swarm theory. In: Proceedings of the sixth international symposium on micro machine and human science. Vol. 1, New York (NY); p. 39–43.
- Elazab A, Wang C, Jia F, Wu J, Li G, Hu Q. 2015. Segmentation of brain tissues from magnetic resonance images using adaptively regularised kernel-based fuzzy-means clustering. *Comput Math Methods Med.* 2015:1–12.
- Gertych A, Pietka E, Liu BJ. 2007. Segmentation of regions of interest and post-segmentation edge location improvement in computer-aided bone age assessment. *Pattern Anal Appl.* 10(2):115–123. doi:10.1007/s10044-006-0056-4.
- Gilsanz V, Ratib O. 2005. Hand bone age: a digital atlas of skeletal maturity. Springer Science & Business Media.
- Giordano D, Leonardi R, Maiorana F, Scarciofalo G, Spampinato C. 2007. Epiphysis and metaphysis extraction and classification by adaptive thresholding and dog filtering for automated skeletal bone age analysis. In: 2007 29th Annual International Conference of the IEEE Engineering in Medicine and Biology Society. Aug 22–26; Lyon, France: IEEE; p. 6551–6556.
- Giordano D, Spampinato C, Scarciofalo G, Leonardi R. 2010. An automatic system for skeletal bone age measurement by robust processing of carpal and epiphysal/metaphysal bones. *IEEE Trans Instrum Meas.* 59(10):2539–2553.
- Gong M, Tian D, Su L, Jiao L. 2015. An efficient bi-convex fuzzy variational image segmentation method. *Inf Sci.* 293:351–369. <http://www.sciencedirect.com/science/article/pii/S0020025514009293>.
- Gonzalez W, Woods RE. 2004. Eddins, digital image processing using MATLAB. 3rd ed. Prentice Hall.
- Greulich WW, Pyle SI. 1959. Radiographic atlas of skeletal development of the hand and wrist. *Am J Med Sci.* 238(3).
- Güraksin GE, Uğuz H, Baykan ÖK. 2016. Bone age determination in young children (newborn to 6 years old) using support vector machines. *Turkish J Electr Eng Comput Sci.* 24(3):1693–1708.
- Hartigan JA, Wong MA. 1979. Algorithm as 136: A k-means clustering algorithm. *J R Stat Soc Ser C (Appl Stat).* 28(1):100–108.
- Hsieh C, Chen C, Jong T, Liu T, Chiu C. 2012. Automatic segmentation of phalanx and epiphyseal/metaphyseal region by gamma parameter enhancement algorithm. *Meas Sci Rev.* 12(1):21–27.
- Hum YC. 2013. Segmentation of hand bone for bone age assessment. Springer. doi:10.1007/978-981-4451-66-6.
- Kashif M, Deserno TM, Haak D, Jonas S. 2016. Feature description with sift, surf, brief, brisk, or freak? a general question answered for bone age assessment. *Comput Biol Med.* 68:67–75. <http://www.sciencedirect.com/science/article/pii/S0010482515003741>.
- Kashif M, Jonas S, Haak D, Deserno TM. 2015. Bone age assessment meets SIFT. *Proc SPIE.* 941439–941439–7. doi:10.1117/12.2074572.
- Lee JM, Kim WY. 2008. Epiphyses extraction method using shape information for left hand radiography. In: International Conference on Convergence and Hybrid Information Technology, 2008. ICHIT '08. Aug 28–30; Daejeon, South Korea: IEEE; p. 319–326.
- Li C, Huang R, Ding Z, Gatenby JC, Metaxas DN, Gore JC. 2011. A level set method for image segmentation in the presence of intensity inhomogeneities with application to mri. *IEEE Trans Image Process.* 20(7):2007–2016.
- Liu Z, Chen J, Jian L, Yang L. 2007. Automatic bone age assessment based on pso. In: 2007 1st International Conference on Bioinformatics and Biomedical Engineering. Jul 6–8; Wuhan, China: IEEE; p. 445–447.
- Manos G, Cairns A, Rickets I, Sinclair D. 1994. Segmenting radiographs of the hand and wrist. *Comput Methods Program Biomed.* 43(3):227–237.
- Michael DJ, Nelson AC. 1989. Handx: a model-based system for automatic segmentation of bones from digital hand radiographs. *IEEE Trans Med Imaging.* 8(1):64–69.
- Orlando JI, Prokofyeva E, Blaschko MB. 2017. A discriminatively trained fully connected conditional random field model for blood vessel segmentation in fundus images. *IEEE Trans Biomed Eng.* 64(1):16–27.
- Osher S, Sethian JA. 1988. Fronts propagating with curvature-dependent speed: algorithms based on hamilton-jacobi formulations. *J Comput Phys.* 79(1):12–49. <http://www.sciencedirect.com/science/article/pii/0021999188900022>.
- Otsu N. 1979. A threshold selection method from gray-level histograms. *IEEE Trans Syst Man Cybern.* 9(1):62–66.
- Pappas TN, Jayant NS. 1988. An adaptive clustering algorithm for image segmentation. In: Second International Conference on Computer Vision. 1988 Dec 5–8; Tampa (FL): IEEE; p. 310–315.
- Park KH, Lee JM, Kim WY. 2007. Robust epiphyseal extraction method based on horizontal profile analysis of finger images. In: International Symposium on Information Technology Convergence, 2007. ISITC 2007. Nov 23–24; Joenju, South Korea: IEEE; p. 278–282.
- Perona P, Malik J. 1990. Scale-space and edge detection using anisotropic diffusion. *IEEE Trans Pattern Anal Mach Intell.* 12(7):629–639.
- Pietka E, Gertych A, Pospiech S, Cao F, Huang HK, Gilsanz V. 2001. Computer-assisted bone age assessment: image preprocessing and epiphyseal/metaphyseal roi extraction. *IEEE Trans Med Imaging.* 20(8):715–729.
- Pietka E, Pospiech-Kurkowska S, Gertych A, Cao F. 2003. Integration of computer assisted bone age assessment with clinical {PACS}. *Comput Med Imaging Graphics.* 27(23):217–228. <http://www.sciencedirect.com/science/article/pii/S0895611102000769>.
- Seok J, Kasa-Vubu J, DiPietro M, Girard A. 2016. Expert system for automated bone age determination. *Expert Syst Appl.* 50:75–88. <http://www.sciencedirect.com/science/article/pii/S0957417415008131>.
- Sharif BS, Zaroug SA, Chester EG, Owen JP, Lee EJ. 1994. Bone edge detection in hand radiographic images. In: Engineering in Medicine and Biology Society, 1994. Engineering Advances: New Opportunities for Biomedical Engineers. Proceedings of the 16th Annual International Conference of the IEEE. Vol. 1. Nov 3–6; Baltimore (MD): IEEE; p. 514–515.
- Simu S, Lal S. 2017. A study about evolutionary and non-evolutionary segmentation techniques on hand radiographs for bone age assessment. *Biomed Signal Process Control.* 33:220–235.
- Spampinato C, Palazzo S, Giordano D, Aldinucci M, Leonardi R. 2017. Deep learning for automated skeletal bone age assessment in x-ray images. *Med Image Anal.* 36:41–51. <http://www.sciencedirect.com/science/article/pii/S1361841516301840>.
- Tanner J, Healy M, Goldstein H, Cameron N. 2001. Assessment of skeletal maturity and prediction of adult height: TW3 method. Philadelphia: Saunders.
- Thangam P, Thanushkodi K, Mahendiran T. 2012. Pso for graph-based segmentation of wrist bones in bone age assessment. *Int J Comput Commun Control.* 8(1):153–160. <http://univagora.ro/jour/index.php/ijccc/article/view/179>.
- Trist-Vega A, Arribas JI. 2008. A radius and ulna TW3 bone age assessment system. *IEEE Trans Biomed Eng.* 55(5):1463–1476.
- UNICEF. 2011. The situation of children in India: a profile. New Delhi: United Nations Childrens Fund/India.